# Physical Aging in Polymer and Polymer Nanocomposite Glasses

by

Amy Liu

B.Sc., The University of British Columbia, 2007

A THESIS SUBMITTED IN PARTIAL FULFILLMENT OF
THE REQUIREMENTS FOR THE DEGREE OF

Master of Science

in

The Faculty of Graduate Studies

(Physics)

The University of British Columbia

(Vancouver)

December 2009

# Abstract

Physical aging in polymer glasses is a nonequilibrium phenomenon characterized by spontaneous processes that lead to changes in almost all physical properties. While all glasses undergo physical aging, polymer glasses are among the most widely used glasses in research and engineering due to their good glass-forming properties and wide applications. This master's thesis uses molecular dynamics (MD) simulations to explore recently observed experimental phenomena related to physical aging in polymer glasses and polymer nanocomposites. Two manuscripts (published and to be published) have been produced in the duration of this work and are included in chapters 2 and 3.

The first manuscript focuses on the effect of mechanical stresses on physical aging in polymer glasses. This is a complicated and controversial subject as experimental observations have provided evidence both for and against mechanical rejuvenation and overaging. Specifically, we use MD simulations on a coarse-grained bead spring model to investigate the stress-enhanced yielding of polymer glasses. Understanding the origin of this behavior will not only verify whether this can be considered as an example of mechanically induced overaging; it will facilitate the development of more realistic constitutive relations for the yield response of glassy polymers, a subject that has been awarded considerable attention in the last few decades.

The second manuscript is concerned with a relatively new area of research, which involves altering the aging behavior of polymer glasses with the addition of nanoscopic fillers. These polymer nanocomposite systems are difficult to explore due to the complicated interactions between the fillers and the polymer matrix. Unfortunately, limited experimental work (and no simulation work known to the author) have been devoted to investigating the physical aging properties of these systems. In this work, we attempt to develop a coarse-grained polymer nanocomposite MD model to study the impact of nanoparticles on the physical aging behavior of glassy polymers.

This thesis should motivate the use of simulations in conjunction with experiments when studying physical aging in glasses.

# Table of Contents

# List of Figures

# Acknowledgements

First, I would like to thank my supervisor Jörg Rottler not only for his time, patience and knowledge, but also for his constant encouragement throughout the duration of my degree. I would also like to thank my colleagues Parmveer, Adam, Martha, Ramandeep, Anand and Justin for their friendship and support, and especially Mya for countless helpful discussions.

# Statement of Co-Authorship

The manuscript chapters (2-3) were co-written with Jörg Rottler. I was responsible for carrying out the research under the guidance of Professor Rottler. I also carried out the simulation experiments and data analysis presented in this dissertation.

# Chapter 1

# Introduction

## 1.1 Physical Aging in Polymer Glasses

### 1.1.1 Introduction to Glasses

Glasses (or amorphous structures) are materials with no long range order. The highly disordered arrangement of atoms leads to the lack of periodicity throughout the system and results in liquid-like configurations. The dynamics of these materials, however, are surprisingly solid-like. For example, the resistance to shear is a property that glasses possess but is characteristic of solids. The nature of the unique structure and properties of glass is not clearly understood, and its wide range of applications makes for one of the most active areas of research.

A brief background on the formation of a glass is provided in Fig. 1.1. When a material cools from its liquid state to its melting temperature $T_m$, the system can either undergo a drastic shrinkage in volume (or increase in density) and crystallize or it can continue to cool past its melting temperature with relatively slow, continuous change in volume into a super-cooled state. The mobility of the atoms decreases until the glass transition temperature $T_g$, which can be defined as the intersection of lines tangent to the high and low temperature dependencies, as shown in Fig. 1.1. The resulting solid-like structure is known as glass. This transition is much more complicated than the conventional liquid-crystal transition in many ways. For example, there is no precise distinction between the glassy and supercooled states, and the value of $T_g$ is dependent on the system's thermomechanical history (eg. cooling rates). Also, the lack of long range order means that none of the known singularities associated with liquid-solid phase transitions can be applied to the glass transition [1]. The nature of the glass transition remains an active and controversial area of research. This work does not focus on the glass transition; rather, it focuses on what happens below $T_g$, in the glassy regime. Here, the glass continues to explore its configuration space but never quite reaches equilibrium (at least relative to experimental
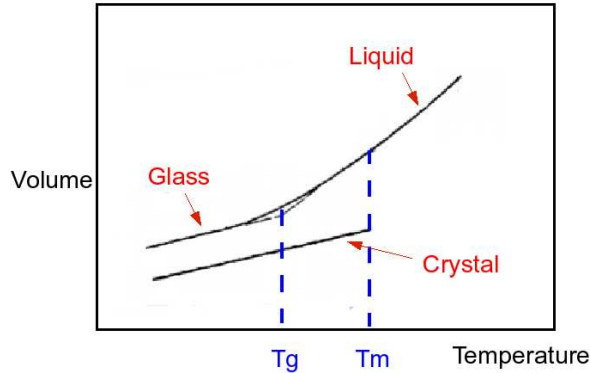
Figure 1.1: The glass transition demonstrated through change in volume vs temperature. The conventional liquid to crystal transition (which involves a drastic shrinkage in volume due to freezing) is also shown on the bottom.

timescales). This results in physical properties that depend on the time since vitrification, or waiting time $t_w$. This phenomenon is known as physical aging. We will only consider physical aging polymer glasses, which are structural glasses widely used in research and also have an extensive list of applications.

Physical aging can be witnessed not only in structural glasses [2], but also in spin [3], electron [4], vortex [5] and other more exotic types of glasses. While significant research efforts have been made towards a unifying description of aging in glasses [1, 6, 7], this remains a challenge. This work contributes to this effort by using computer simulations to explore the molecular level details of some of the phenomena observed in experiments with aging polymer glasses and polymer nanocomposites.

## 1.1.2 Manifestations of Physical Aging

All polymer glasses undergo physical aging, and the resultant changes in physical properties with time can have detrimental effects on the fracture toughness and lifetime to failure of these materials. Understanding aging in polymer glasses will bring prospects of being able to predict and control the effect of aging, leading to the development of high performing and long lasting glasses. One of the reasons aging in glasses is such a difficult subject to understand is the fact that aging can manifest itself in many distinct ways. In this section, we provide the background for a few important examples which are relevant to this work.
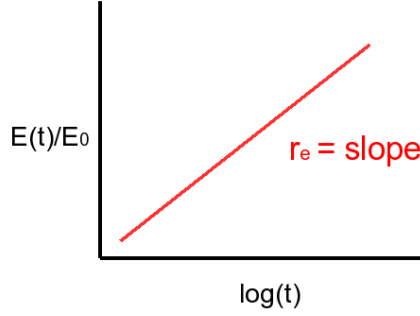
Figure 1.2: Extraction of physical aging rate $r_e$ from the linear dependence of energy on logarithmic physical aging time.

In the glassy regime, dynamics are highly constrained and only small structural relaxations can take place, leading to a slow evolution of thermodynamic quantities such as internal energy, enthalpy and density. This leads to the first manifestation of aging we will introduce here, which is the linear dependence of these quantities on logarithmic physical aging time. This is shown schematically in Fig. 1.2. For example, one can define the physical aging rate from the change in energy:

$$r_e = \frac{1}{E_0} \frac{dE}{d\log(t)} \tag{1.1}$$

the same quantity can also be defined for volume and enthalpy. This macroscopic physical aging rate has been used extensively as a way of evaluating physical aging in glasses [8].

The fact that physical properties of aging glasses change depending on the time since vitrification also results in memory effects. This leads to another manifestation of aging, where structural relaxation times increase as a power law $\tau_\alpha \sim t_w^\mu$, and $\mu$ is defined as the aging exponent. This is most typically demonstrated in observations of the mechanical creep response [9], where samples aged for different waiting times $t_w$ are subjected to a constant load $\sigma$, and the resultant strain $\epsilon(t, t_w)$ is measured. The creep compliance $J(t, t_w) = \frac{\epsilon(t,t_w)}{\sigma}$ curves can be shifted along the time axis with shift factors $a$ to collapse onto a single master curve as shown in Fig. 1.3. These shift factors obey a power law relation $a \sim t_w^{-\mu}$. In molecular simulations, the same protocol can be applied to the microscopic mean-squared displacement for different $t_w$:

3
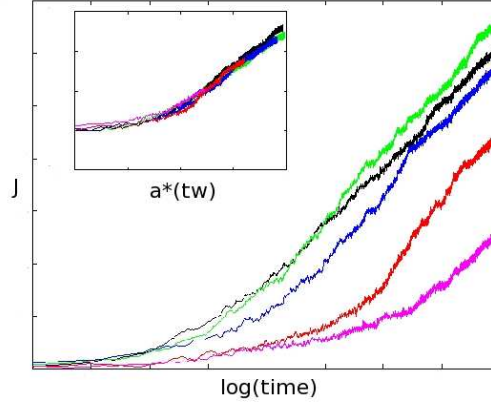
Figure 1.3: Creep compliance $J(t, t_w)$ obtained from MD simulations of a polymer glass for 5 different $t_w$. Inset shows curves for all $t_w$ shifted along the time axis (with shift factors $a$) to collapse onto a single master curve.

$$\langle \Delta \mathbf{r}(t, t_w)^2 \rangle = \frac{1}{N} \sum_{j=1}^{N} \left( \mathbf{r}_j(t) - \mathbf{r}_j(t_w) \right)^2 \tag{1.2}$$

where $r_j$ denotes the position of particle $j$. In fact, it was shown in ref. [10] that the resultant aging exponents $\mu$ are comparable for the macroscopic mechanical creep response and microscopic mean-squared displacement as the two both depend on the same microscopic rearrangements.

The third manifestation of aging that will be presented here is related to the yield behavior of polymer glasses. Yielding occurs when the glass subject to stress switches from deforming elastically to plastically, as can be seen in the stress-strain curve shown in Fig. 1.4. The yield stress can be defined as the maximum of this stress-strain curve, and it is dependent on the history of the material. For polymer glasses aged for different $t_w$ and subsequently strained, it has been shown that the resultant yield stress increases with $t_w$ [11, 12]. This trend is also demonstrated in Fig. 1.4.

## 1.1.3 Effect of Mechanical Deformation on Physical Aging

As mentioned in the previous section, aging can manifest itself in changes in mechanical properties. It has also been shown experimentally that mechanical deformation
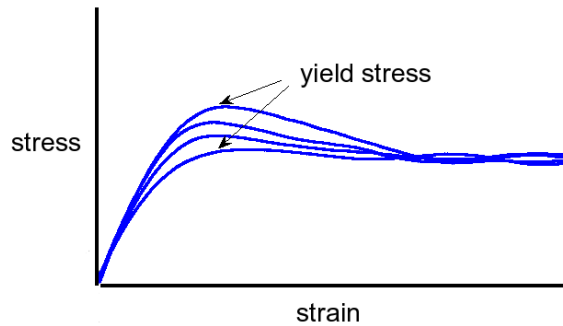
Figure 1.4: Stress-strain curves obtained from MD simulations of a polymer glass under uniaxial stress for 4 $t_w$. The sample deforms elastically until the yield point, after which it deforms plastically. The yield stress is shown to increase with increasing $t_w$.

can alter the aging dynamics, and these effects can be quite contradicting. For example, using creep compliance measurements $J(t, t_w)$ of structural glasses, Struik showed that the application of sub-yield stresses can reduce the evolution of relaxation times (or reduce the aging exponent $\mu$) as to "rejuvenate" the glass [9]. However, Lee and McKenna showed by studying the physical aging response of epoxy glass, that while $\mu$ does decrease with increasing applied stress, the time $t^*$ for the glass to recover towards mechanical equilibrium is unchanged [13]. This finding contradicts the rejuvenation hypothesis, which suggests that $t^*$ should increase with increasing applied stress. In addition, others have shown that mechanical deformation can actually have "overaging" effects [14–16]. For example, Klompen et al. showed that the increase in yield stress with waiting time is enhanced for polymer glasses that are aged under load [17]. These apparent contradictions are consequences of the lack of consistent interpretations for rejuvenation and overaging. Unfortunately to this day, there is no clear picture of the underlying structure and energetic mechanisms that takes place as a result of mechanical deformation [18]. We will show that one of the contradictions can be resolved by using simulations to explore the molecular level details of the system.

## 1.2  Shear Yielding in Polymer Glasses

Understanding and predicting the yield behavior of polymer glasses is of great importance for the preformance and reliability of polymeric materials. While it is known that the yield stress depends on temperature, deformation rate, loading conditions and material history, the relations are complicated and it remains a great challenge to develop a unifying relation that can model realistically the yield behavior as a function of all of these factors. Significant progress has been made in terms of constructing constitutive relations that model the effect of temperature and history on the evolution of yield stress [11, 17, 19]. However, the effect of mechanical deformation on the yield behavior is much more complicated and controversial than that of temperature as a consequence of the complex interplay between aging and mechanical deformation described in the previous section.

New behaviors continue to be observed for different polymers subject to different thermomechanical histories. While it is difficult to model all the specifics of these effects, one can study simpler types of mechanical deformations at constant strain rates and temperatures. This will provide clues as to how to progress towards a more complete and realistic constitutive model. We shall now focus on one such simple scenario: a polymer glass aged at fixed temperature for different waiting times, after which uniaxial tension/compression is applied at a constant strain rate to determine the resultant yield stress. For samples that are not aged under stress, it has been shown that yield stress increases with time since vitrification. This increase is due to physical aging and is the effect of the relocation on the energy landscape to a new higher energy state. This is a well known manifestation of aging (see section 1.1.2) and has been incorporated into many existing constitutive models [11, 17]. A more recent effort studying the effect of thermomechanical treatments on the evolution of yield stress found that the yield stress is further increased with samples that are aged under load, and that this effect is enhanced for larger loads. These trends are demonstrated in Fig. 1.5; the yield stress for the sample aged under load (solid red) increases much faster with respect to $t_w$ than the sample aged under no load (dashed blue).

A first attempt to model this behavior introduced aging kinetics into existing 3D elastoviscoplastic constitutive models, and it was found that one can derive appropriate shift functions to fit this behavior [17]. However, the origin of this enhancement in yield stress remains unknown, and it is unclear whether it can be interpreted as a form
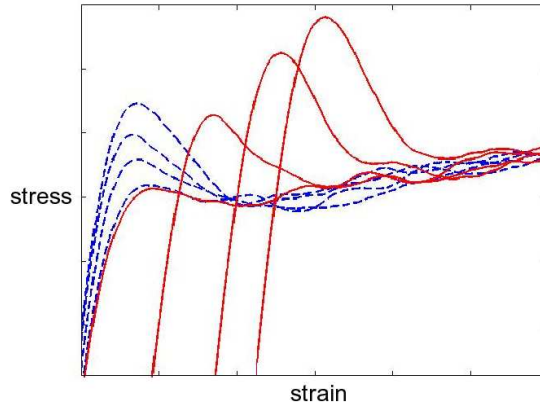
Figure 1.5: Stress-strain curves obtained from MD simulations of polymer glasses for 4 $t_w$ with no pre-stress (dashed blue) and with finite pre-stress (solid red). One can see that the increase in yield stress with respect to $t_w$ is enhanced for the case with finite pre-stress relative to the case with no pre-stress.

of "overaging" caused by mechanical deformation (ie. whether it involves relocation on the energy landscape). In chapter 2, we use molecular dynamics (MD) simulations of a simple bead-spring polymer glass model to explore the origin of this effect, and attempt to verify whether this is evidence for deformation induced overaging.

## 1.3 Aging in Confined Glasses

In addition to mechanical deformation, there are also other ways to alter the aging process. For example, it is well known that the properties of confined glasses can deviate substantially from those of bulk samples [20]. The introduction of interfaces plays a critical role in a wide range of polymer applications such as thin films, coatings, lubricants, adhesives [21], and is a subject of many research efforts. For example, confinement effects on the glass transition temperature in thin polymer films have been studied extensively in experiments [22–24] as well as simulations [25–27]. These results indicate that the value of $T_g$ near interfaces can be significantly altered depending on the type of interfacial interactions. Even though much less work has been devoted to studying the effect of confinement on the aging behavior, existing experimental results show that the physical aging rate near interfaces can also differ significantly from those found in the bulk regions [28]. For example, Priestley et al.

showed that physical aging rates can be suppressed near the surface of an attractive interface [29]. The properties of the interfacial area are inherently difficult to explore, and little detail is known about the dynamics at the interface. Fortunately, much of these difficulty can be overcome with the use of simulations, making it a popular theoretical approach for the study of interfaces in polymers. It is important to understand the effect of confinement on aging as the introduction of interfaces into the polymer matrix has the potential of becoming an effective way of controlling the aging process in polymer glasses.

### 1.3.1 Polymer Nanocomposites

In recent years, the ability to make nano-scale fillers has provided opportunities for the development of high-performance multifunctional nanocomposites [20]. For example, the addition of nanoparticles to polymer systems has demonstrated significant enhancements in mechanical properties over the parent polymer system. These polymer nanocomposite (PNC) systems have also been found to develop new electrical and thermal properties that are not observed in traditional micron-size fillers [30]. The large surface area of these nano-scale additives leads to large volume fraction of interfacial polymer compared to volume fraction of fillers, and the interfacial region can have very different properties compared to the original polymer matrix. In addition, the small size of the nanoparticles have also been shown to result in polymer composites with enhanced ductility and toughness compared to micrometer-scale fillers as they are an order of magnitude smaller than the critical crack size [31, 32].

Nanofillers have an advantage over larger fillers or films as one can alter significantly the properties of the entire polymer matrix using a very small volume percentage of well-dispersed nanofillers. However, nanocomposite systems are more complicated than thin films as inconsistencies in the size, geometry and dispersion of the nanoscopic fillers can make it very difficult to understand and predict their effects [30, 33].

Limited work has been done on studying physical aging in nanocomposites. Experiments using poly(2-vinyl pyridine) (P2VP) containing silica and alumina nanoparticles (which form strongly attractive hydrogen-bonds with the polymer chains) found significant suppression of physical aging rate compared to the neat P2VP system [34]. However, a study measuring the creep compliance of Polyamide 6 nanocomposites (polymer nanocomposite containing layered silicate particles which form ionic bonds

with the polymer chains) reported no change in relaxation times [35]. With such limited experimental work studying different manifestations of aging with different systems, it is difficult to make any conclusive statements about the underlying effect on aging brought about by the presence of nanofillers. Here one can greatly benefit from the use of simulations, which allows for systematic and consistent measurements of the microscopic and macroscopic dynamics, as well as simultaneous explorations of different manifestations of aging.

Chapter 3 presents a simulation model that we developed for a polymer-nanocomposite system to study the effect of nanospherical additives on the aging behavior of polymer glasses. This model is similar to the one used in ref. [36]. The hope is to have a simple coarse-grained model that will contain some of the qualitative features observed in experiments, and can be used to probe the microscopic quantities that are not easily accessible in experiments. We also study simultaneously the macroscopic physical aging rate as well as the change in structural relaxation times of the microscopic mean-squared displacements.

## 1.4 Molecular Dynamics Simulations

In the last three decades, MD simulations have emerged as a powerful research tool for the study of glassy dynamics. MD consists of finding the trajectory of all particles by solving numerically, step-by-step, Newton's classical equations of motion:

$$\dot{\mathbf{r}}_i = \frac{\mathbf{p}_i}{m_i} \qquad \text{and} \qquad \dot{\mathbf{p}}_i = \mathbf{f}_i \tag{1.3}$$

where $\mathbf{r}^N = (\mathbf{r}_1, \mathbf{r}_2, \ldots, \mathbf{r}_N)$, $\mathbf{f}^N = (\mathbf{f}_1, \mathbf{f}_2, \ldots, \mathbf{f}_N)$ and $\mathbf{p}^N = (\mathbf{p}_1, \mathbf{p}_2, \ldots, \mathbf{p}_N)$ are the atomic coordinates, forces and momenta respectively ($m$ is the atomic mass). The typical numerical algorithm used in MD is Velocity Verlet:

$$
\begin{aligned}
\mathbf{p}_i(t + \tfrac{1}{2}\delta t) &= \mathbf{p}_i(t) + \tfrac{1}{2}\delta t \mathbf{f}_i(t) \\
\mathbf{r}_i(t + \delta t) &= \mathbf{r}_i(t) + \delta t \mathbf{p}_i(t + \tfrac{1}{2}\delta t)/m_i \\
\mathbf{p}_i(t + \delta t) &= \mathbf{p}_i(t + \tfrac{1}{2}\delta t) + \tfrac{1}{2}\delta t \mathbf{f}_i(t + \delta t)
\end{aligned}
$$

which has the advantage of being symplectic, time-reversible and second order accu-

rate. The fact that only one force evaluation per step is required makes it a rather inexpensive method.

Even though the concepts used in MD simulations are simple, the implementation can be quite complicated due to the large number of coupled equations and constraints involved. Fortunately, software packages like LAMMPS (Large-scale Atomic/Molecular Massively Parallel Simulator, see http://lammps.sandia.gov for more information) abstract away most or the details and complications associated with MD simulations. However, even with efficient large scale simulators like LAMMPS, MD is computationally expensive, which severely limits the time scale and system sizes that can be simulated. It is therefore very important to use the simplest models that can faithfully represent the essential physics.

For simulation of the polymer glasses used in this work, we employ a coarse grained model used extensively in studies of glassy dynamics [21, 27, 37]. This model was proposed by Grest and Kremer in 1990 and essentially models the polymer atoms as simple beads connected by stiff springs [37]. The pair-wise van der Waals forces between the beads are modeled by the Lennard-Jones (LJ) potential:

$$V_{\mathrm{LJ}}(r) = 4\epsilon \left[ \left( \frac{\sigma}{r} \right)^{12} - \left( \frac{\sigma}{r} \right)^{6} \right] \qquad \text{for } r < r_c \tag{1.4}$$

where $\sigma$ represents the diameter of the atoms and $\epsilon$ is the well depth. The minimum of the LJ potential occurs at $r = 2^{1/6}\sigma$. $r_c$ is the cut-off distance beyond which the potential is set to zero. It is usually set to $2.5\sigma$ to save computational time but can also be used to tune the pair-pair interaction (for example, setting $r_c$ right at the minimum $2^{1/6}\sigma$ results in a purely repulsive interaction). The intra-molecular covalent bonds are typically represented using a combination of the LJ potential and the finitely-extensible non-linear elastic (FENE) potential:

$$V_{\mathrm{FENE}}(r) = \begin{cases} -\frac{1}{2}kR_0^2 \ln(1 - \frac{r}{R_0}^2) & r < R_0; \\ \infty & r \geq R_0 \end{cases} \tag{1.5}$$

The fact that this potential cannot be extended beyond $r = R_0$ ensures that the chains cannot overlap or move through one another. The minimum for this covalent bond model (FENE + LJ) is about $0.96\sigma$. The competition between the equilibrium lengths of the pair-wise and bond potential is what prevents the polymer from ordering and forming crystalline structures, making this a good glass-forming model.

Unlike the bead-spring model described above for pure polymer systems, no com-

monly accepted coarse-grained model exists for modeling PNC systems. While many simulation models have been developed for studying the behaviors of polymers containing nanoparticles, none of the models known to the author have been used to study the aging behavior. For example, Vacatello et al. use Monte Carlo simulations of polymer melts containing spherical entities to study the arrangement of the chain segments near the interfaces [38]. Papakonstantopoulos et al. also use a Monte Carlo approach to study the changes in mechanical behavior resulting from perturbation of nanoparticles [33]. Starr et al. employ MD simulations of a single polygonic particle containing force sites to study the effect of the particle on the glass transition temperature of the polymer matrix it is immersed in [36].

The model we developed for studying aging in PNCs is similar to the one used by Starr et al.: 10 to 20 spherical "nanoparticles" (corresponding to 6 to 10 volume percent) are introduced into a bead-spring polymer system. Each nanoparticle is covered with interaction sites on the vertices resulting from the tessellation of each sphere's surface (see Fig. 3.1(a) for an illustration and section 3.2 for more detail). The interaction between the sites and the polymer atoms are modeled using the LJ potential and are tuned by altering the parameters $\epsilon$ and $r_c$.

Another important component of MD simulations is to control the temperature and pressure of the simulation environment. For example, the Nose-Hoover algorithm does this by introducing the effect of an external heat reservoir with additional degrees of freedom, and then using the interaction between the heat reservoir and the system to control the exchange of kinetic energy between them [39, 40]. The Langevin algorithm on the other hand adjusts the kinetic energy of the particles by adding a frictional force that is proportional to the velocity [40]. LAMMPS provides commands that automate most of the thermostatic/barostatic algorithms. One does need to set parameters such as the time scale on which pressure/temperature is relaxed to ensure that the system evolves in a smooth and controlled fashion. This is especially important during the annealing process as well as when applying external stresses to the system.

# References

[1] W. Gotze and L. Sjogren. Relaxation processes in supercooled liquids. *Rep. Prog. Phys*, 55:241, 1992.

[2] L. Cipelletti and L. Ramos. Slow dynamics in glassy soft matter. *J. Phys.: Condens. Matter*, 17:R253, 2005.

[3] L. Lundgren, P. Svedlindh, P. Nordblad, and O. Beckman. Dynamics of the relaxation-time spectrum in a CuMn spin-glass. *Phys. Rev. Lett.*, 51:911, 1983.

[4] A. Vaknin and Z. Ovadyahu. Aging effects in an Anderson insulator. *Phys. Rev. Lett.*, 84:3402, 2000.

[5] X. Du, G. Li, E. Andrei, M. Greenblatt, and P. Shuk. Ageing memory and glassiness of a driven vortex system. *Nature Physics*, 3:111, 2007.

[6] F. Ritort. Glassiness in a model without energy barriers. *Phys. Rev. Lett.*, 75:1190, 1995.

[7] C. Monthus and J. P. Bouchaud. Models of traps and glass phenomenology. *J. Phys. A: Math. Gen.*, 29:3847, 1996.

[8] J. M. Hutchinson. Physical aging of polymers. *Prog. Polym. Sci.*, 20:703–760, 1978.

[9] L. C. E. Struik. *Physical aging in amorphous polymers and other materials.* Elsevier, Amsterdam, 1978.

[10] M. Warren and J. Rottler. Simulations of aging and plastic deformation in polymer glasses. *Phys. Rev. E,* 76:031802, 2007.

[11] O. A. Hasan, M. C. Boyce, X. S. Li, and S. Berko. An investigation of the yield and postyield behavior and corresponding structure of poly(methyl methacrylate. *J. Poly. Sc. Part B: Polym. Physics*, 31:185, 1993.

[12] A. L. Volynskii, A. V. Efimov, and N. F. Bakeev. Structural aspects of physical aging of polymer glasses. *Polymer Science Series C*, 49:301, 2007.

[13] A. Lee and G. B. McKenna. The physical aging response of an epoxy glass subjected to large streses. *Polymer*, 31:423, 1990.

[14] P. I. Vincent. The necking and cold-drawing of rigid plastics. *Polymer*, 1:7, 1960.

[15] L. C. E. Struik. The mechanical enhancement of physical aging. *Polymer*, 21:962, 1980.

[16] Y. Nanzai, A. Miwa, and S. Z. Cui. Aging in fully annealed and subsequently strained poly(methyl methacrylate). *Polym. J.*, 32:51, 2000.

[17] E. T. J. Klompen, T. A. P. Engels, L. E. Govaert, and H. E. H. Meijer. Modeling of the postyield response of glassy polymers: influence of thermomechanical history. *Macromolecules*, 38:6997, 2005.

[18] G. B. McKenna. Mechanical rejuvenation in polymer glasses: fact or fallacy? *J. Phys.: Condens. Matter*, 15:S737–S763, 2003.

[19] J. Rottler and M. O. Robbins. Yield conditions for deformation of amorphous polymer glasses. *Phys. Rev. E*, 64:051801, 2001.

[20] L. Schadler, L. Brinson, and W. Sawyer. Polymer nanocomposites: a small part of the story. *JOM*, 59:2007, 2007.

[21] K. Binder (Eds). *Monte Carlo and molecular dynamics simulations in polymer science.* Oxford, 1995.

[22] J. Keddie, R. Jones, and R. Cory. Size-dependent depression of the glass transition temperature in polymer films. *Europhys. Lett.*, 27:59, 1994.

[23] J. Forrest and K. Dalnoki-Veress. The glass transition in thin polymer films. *Advances in Colloid and Interface Science*, 94:167, 2001.

[24] C. Ellison and J. M. Torkelson. The distribution of glass-transition temperatures in nanoscopically confined glass formers. *Nature Materials*, 10:695, 2003.

[25] J. Torres, P. Nealey, and J. de Pablo. Molecular simulation of ultrathin polymeric films near the glass transition. *Phys. Rev. Lett.*, 85:3221, 2002.

[26] A. Baljon, M. Van Weert, R. Degraaff, and R. Khare. Glass transition behavior of polymer films of nanoscopic dimensions. *Macromolecules*, 38:2391, 2005.

[27] J. Baschnagel and F. Varnik. Computer simulation of supercooled polymer melts in the bulk and in confined geometry. *J. Phys.: Condens. Matter*, 17:R851, 2005.

[28] R. Priestley. Physical aging of confined glasses. *Soft Matter*, 5:919, 2009.

[29] R. Priestley, C. Ellison, L. Broadbelt, and J. M. Torkelson. Structural relaxation of polymer glasses at surfaces, interfaces, and in between. *Science*, 309:456, 2005.

[30] T. Ramanathan, S. Stankovich, D. A. Dikin, H. Liu, H. Shen, S. T. Nguyen, and L. C. Brinson. Graphitic nanofillers in pmma nanocomposites - an investigation of particle size and dispersion and their influence on nanocomposite properties. *J. Poly. Sci. Part B:Polymer Physics*, 45:2097, 2007.

[31] B. Ash, R. Siegel, and L. Schadler. Mechanical behavior of alumina/poly(methyl methacrylate) nanocomposites. *Macromolecules*, 37:1358, 2004.

[32] W. Naous, X. Y. Yu, Q. X. Zhang, K. Naito, and Y. Kagawa. Morphology, tensile properties, and fracture toughness of epoxy/Al203 nanocomposites. *J. Poly. Sci. Part A: Polymer Chemistry*, 44:1466, 2006.

[33] G. J. Papakonstantopoulos, M. Doxastakis, P. F. Nealey, J.-L. Barrat, and J. J. de Pablo. Caculation of local mechanical properties of filled polymer. *Phys. Rev. E*, 75:031803, 2007.

[34] P. Rittigstein and J. M. Torkelson. Polymer-nanoparticle interfacial interactions in polymer nanocomposites: confinement effects on glass transition temperature and suppression of physical aging. *J. Poly. Sci.: Part B: Polymer Physics*, 44:2935, 2006.

[35] D. P. N. Vlasveld, H. E. N. Bersee, and S. J. Picken. Creep and physical aging behavior of PA6 nanocomposites. *Polymer*, 46:12539, 2005.

[36] F. W. Starr, T. B. Schroder, and S. C. Glotzer. Effects of a nanoscopic filler on the structure and dynamics of a simulated polymer melt and the relationship to ultrathin films. *J. Chem. Phys.*, 64:021802, 2001.

[37] K. Kremer and G. S. Grest. Dynamics of entangled linear polymer melts: a molecular dynamics simulation. *J. Chem. Phys*, 92:5057, 1990.

[38] M. Vacatello. Monte carlo simulations of polymer melts filled with solid nanoparticles. *Macromolecules*, 34:1946, 2001.

[39] S. Nose. A molecular dynamics method for simulations in the canonical ensemble. *Mol. Phys.*, 52:255, 1984.

[40] D. Frenkel and B. Smit. *Understanding molecular simulation, 2nd Ed.* Academic Press Inc., Orlando, Florida, USA, 2001.

# Chapter 2

# Origin of Stress Enhanced Shear Yielding in Aging Polymer Glasses

1

Understanding and predicting the yield behavior of glassy polymers is of great importance for the performance and reliability of polymeric materials [1, 2]. It is well known that the shear yield stress of glassy polymers is a complicated function of temperature, deformation rate, loading condition and material history. For uniaxial extension at constant strain rate, one finds in both experiments [3–5] and simulations [6] that the maximum (overshoot) stress generally increases with rate and age or waiting time $t_w$ elapsed since vitrification. During physical aging, glassy materials undergo slow relaxation processes that evolve thermodynamic variables such as density and enthalpy. The increased initial resistance to plastic flow with increasing age results from the continuing descent towards lower energy states on the potential energy landscape. However, aging usually increases the amount of strain softening, which leads to instabilities that promote localization (e.g. necking) [1, 7].

Although models have been developed that describe the combined effect of rate, temperature and aging kinetics on the mechanical properties of structural glasses [4, 6, 7], much confusion still revolves around the influence of different thermomechanical histories. Experiments measuring the creep response of polymer glasses after aging indicate that mechanical shift factors and underlying relaxation times are reduced with increasing applied stress, so that the material appears "rejuvenated" [3]. Similarly, it can be shown that mechanical preconditioning by rolling lowers the yield stress and reduces the amount of strain softening [8]. By contrast, recent experiments found that when stress is applied during the aging period, the shear yield stress is enhanced relative to the unstressed material [7], as if the polymer has aged

---

faster. It is tempting to classify this apparently accelerated aging as "overaging", especially since simulations showed that model amorphous solids subjected to a strain cycle can indeed be brought into a regime of lower potential energy [9]. Atomistic simulations also reported such overaging for rapidly quenched samples, while slowly annealed polymers displayed rejuvenation [10]. Several other experimental studies report stress-enhanced aging effects, but their interpretation and consequences for the yielding behavior of polymer glasses remain controversial and poorly understood [5, 11–13].

In this Letter, we employ simulations to determine the molecular level origin of the apparent enhancement of the yield stress of polymer glasses subject to various loading conditions during aging. Molecular dynamics is used to simulate a coarse-grained bead-spring polymer system, which has been used extensively in studies of glassy dynamics [14] and polymer deformation [15]. The beads are bonded via a finite extensible non-linear elastic (FENE) spring and interact via a truncated 6-12 Lennard Jones (LJ) potential $V_{\text{LJ}}(r) = 4u_0 \left[ (a/r)^{12} - (a/r)^6 \right]$ for $r < r_c = 1.5$, where $u_0$ and $a$ set the reference energy and length scale. Results will be given in LJ units, where the reference time scale is $\tau_{LJ} = \sqrt{ma^2/u_0}$. We consider chains of length $N = 30$ and $N = 100$ beads with a total of $\sim 80000$ beads in a cubic box subject to periodic boundary conditions. To form the glass, the polymer is initialized using a random walk process and equilibrated at a melt temperature of $T = 1.2$ before being quenched rapidly to a temperature of $T = 0.2$ (below the glass transition temperature) at constant pressure. Once the polymer glass is formed, a constant uniaxial tensile stress $\sigma_0$ (in the subyield regime) in the $z$-direction is increased quickly and then held constant for various waiting times $t_w$.

After aging, the pre-stress is removed and the simulation box is then subjected to uniaxial stress at a constant true strain rate of $\sim 10^{-4}$. For both pre-stressing during aging and straining at constant rate after aging, the stresses normal to the strain direction are maintained at zero. The yield stress of the polymer glass is taken as the peak of the stress overshoot portion of the resultant stress-strain curves. Fig. 2.1(a) shows stress-strain curves corresponding to this protocol for four different $t_w$ and tensile deformation in the z-direction. One can see that the yield stress always increases with increasing age, but the polymer glass that was aged under load (red dotted line) shows an enhanced change in yield stress with respect to waiting time compared to the one with no pre-stress (blue solid line). Moreover, this increase in
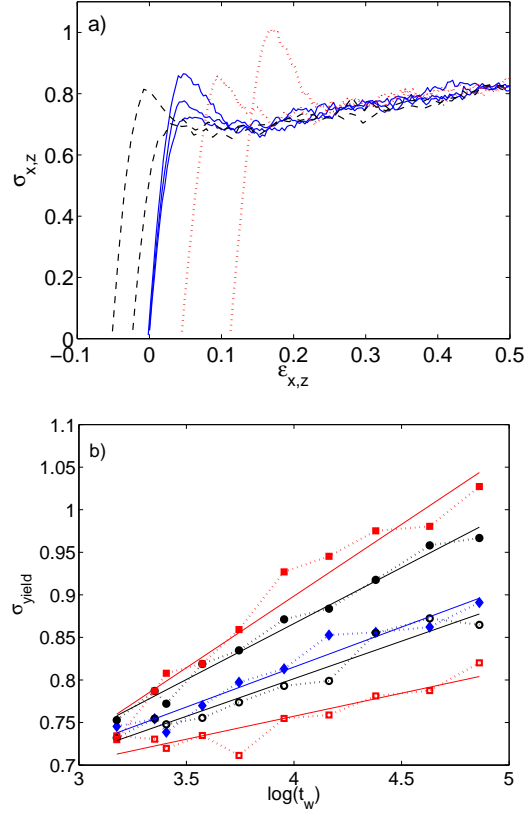
Figure 2.1: (a) Stress in polymer glasses ($N = 100$) for $t_w = 0, 4050$ and $71250$ with pre-stresses of $\sigma_0 = 0$ (blue solid) and 0.5 for tensile deformation in the z- (red dotted, parallel to prestress) and x- (black dashed, perpendicular to prestress) direction as a function of total strain (that includes deformation during aging). (b) Resultant yield stresses as a function of $\log(t_w)$ for $\sigma_0 = 0$ ($\blacklozenge$), $\sigma_0 = 0.3$ in the z ($\bullet$) and x ($\circ$) direction, $\sigma_0 = 0.5$ in the z ($\blacksquare$) and x ($\square$) direction.

yield stress is logarithmically proportional to waiting time, and the rate of increase is stronger for larger pre-stresses, as can be seen in Fig. 2.1(b) (solid symbols). These results qualitatively reproduce those reported in ref. [7], where the evolution of the yield stress of polycarbonate was monitored for different loads applied during a very similar aging protocol.

We first explore whether this difference could be due to changes in the physical aging rate. Fig. 2.2 shows the change in the potential energy per particle with respect to logarithmic aging time for six different values of $\sigma_0$. The inset shows the macroscopic physical aging rate defined as the logarithmic slope of energy relaxation $r_E = (dE/d\log(t))/E_0$ [16], where $E_0 < 0$ is the energy at the end of the stress ramp
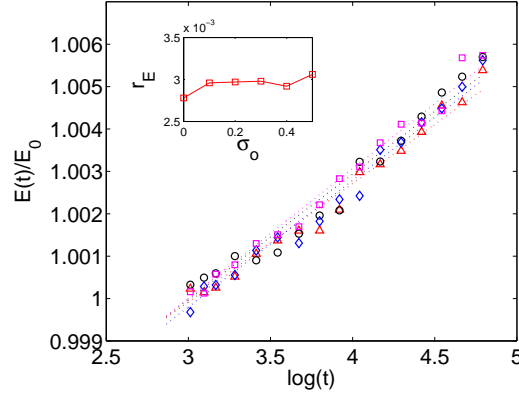
Figure 2.2: Energy relaxation of the polymer glasses ($N = 100$) with pre-stresses of $\sigma_0 = 0$ ($\triangle$), 0.1 ($\circ$), 0.3 ($\diamond$) and 0.5 ($\square$) as a function of aging time. Inset shows the resultant $r_E$ found from the logarithmic slopes.

(similar results are obtained for volume relaxation). Since the physical aging rate does not increase significantly with respect to increasing pre-stress, direct modifications of the aging dynamics are therefore unlikely to be the cause of the non-trivial trends we observe in the yielding behavior.

A large body of work suggests that orientational effects in polymers also lead to modified yield behavior [17–21], but so far has not considered the interplay with aging. Indeed, we find that after aging the system under tensile uniaxial stress $\sigma_0$ in the $z$-direction, the material response has become anisotropic. Fig. 2.1(a) also shows tensile stress-strain curves for the same four $t_w$, but the polymer was strained along the perpendicular x-direction instead (blue dashed line). In stark contrast to the deformation along the z-direction, one can see that the increase of the yield stress with respect to $t_w$ is significantly reduced with respect to the system with no pre-stress. Fig. 2.1(b) summarizes the change in the evolution of yield stress in the direction parallel to the pre-stress (solid markers) and perpendicular to the pre-stress (open markers). The rate of increase of $\sigma_{\text{yield}}$ now decreases with increasing pre-stress.

To quantify this orientation effect, we compute the angle $\cos(\theta)$ between every covalent bond and the z-axis from the projection of the bond vectors onto the strain axis and characterize the degree of polymer alignment through the second Legendre polynomial (Hermans' orientation factor)

$$f_b = \frac{1}{2}(3\langle\cos^2(\theta)\rangle - 1). \tag{2.1}$$

19
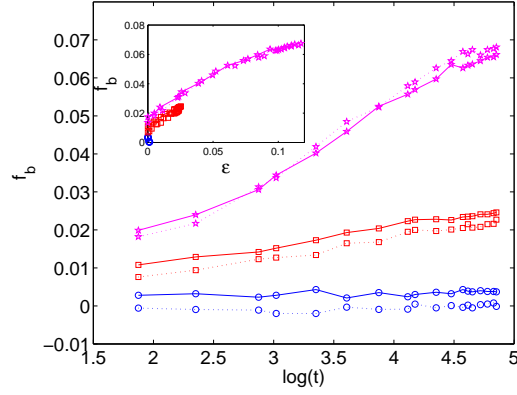
Figure 2.3: Evolution of the orientational order parameter $f_b$ during aging for polymer glasses with pre-stresses of $0(\circ)$, $0.3(\square)$ and $0.5(\star)$. Inset shows $f_b$ as a function of strain $\epsilon$. Same symbols are used for polymers with $N = 100$ (solid line) and $N = 30$ (dotted line).

A value of zero corresponds to random orientations. Experiments often determine $f_b$ from birefringence measurements [20, 21]. An analogous parameter for the orientation of the LJ bonds, $f_{LJ}$, can also be determined by applying a Delaunay triangulation routine to connect nearest neighbor beads, and then finding the projection of the resulting edges onto the z-axis. Fig. 2.3 shows the evolution of $f_b$ during aging. One can see that $f_b$ increases linearly with $\log(t)$ and strain (inset); the rate of change is proportional to $\sigma_0$ and insensitive to chain length, with $f_b$ remaining essentially constant and close to zero for the system with $\sigma_0 = 0$. The secondary (Lennard Jones) bonds orient much less than the covalent bonds, and values of $f_b$ are always an order of magnitude greater than $f_{LJ}$.

To confirm that polymer (re)orientation during aging is in fact responsible for the enhanced rate of change in yield stress, we track the difference in yield stress $\Delta\sigma_{yield}$ between the polymer glass with pre-stress $\sigma_0 = 0.5$ and one with no pre-stress. Fig. 2.4 shows this difference for the total stress $\sigma_{tot}$ at yield, as well as the separate contributions from only the covalent bonds $\sigma_b$ and the LJ interactions $\sigma_{LJ}$ (the thermal contribution is independent of $t_w$ and pre-stress and does not contribute to the difference). Note that even though $\Delta\sigma_{yield}$ is plotted with respect to $\log(t_w)$, this is equivalent to plotting with respect to strain or order parameter $f_b$, since they are proportional to each other (Fig. 2.3).

Fig. 2.4(a) corresponds to tensile/compressive yielding in the direction parallel

20
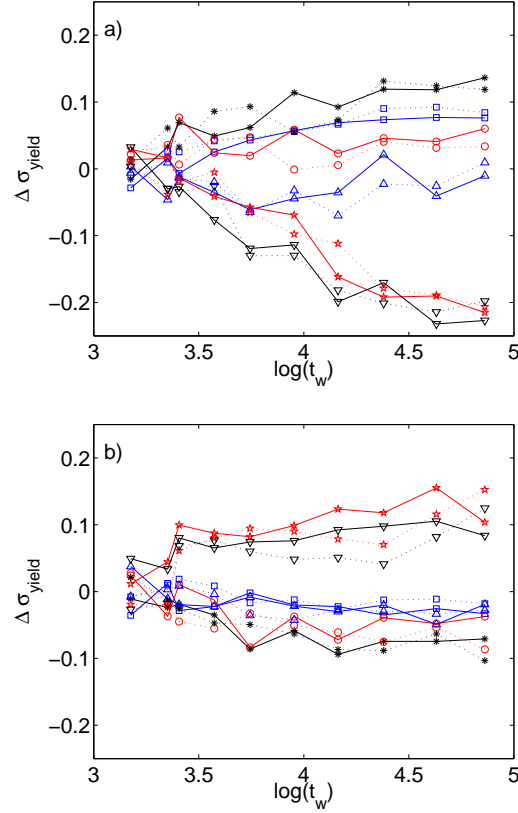
Figure 2.4: Change in shear yield stress for the polymer glass with pre-stress $\sigma_0 = 0.5$ relative to the unstressed polymer. Stress contributions from the covalent bonds, Lennard-Jones interactions and total interactions are shown separately. For tensile strain, $\sigma_b(\square)$, $\sigma_{LJ}(\circ)$, $\sigma_{tot}(*)$ and for compressive strain, $\sigma_b(\triangle)$, $\sigma_{LJ}(\star)$, $\sigma_{tot}(\triangledown)$. Same symbols are used for polymers with $N = 100$ (solid) and $N = 30$ (dotted). Panel (a) shows results for extension and compression along z and (b) shows the same set of data for extension and compression along x.

to the pre-stress. Here the orientation of the covalent bonds is biased towards the straining direction (z-axis), and $f_b$ increases with $t_w$. One can see that $\Delta\sigma_{yield}$ varies almost linearly with respect to $\log(t_w)$ and strain. For tensile strain, $\Delta\sigma_{tot}$ increases with $\log(t_w)$ with most of the contributions coming from the covalent stress $\Delta\sigma_b$. The increase in tensile yield stress is therefore attributable to an increase in projected areal bond density, which is proportional to monomer density and $f_b$. Very different behavior is observed for compressive strain: here $\Delta\sigma_{tot}$ decreases with $\log(t_w)$ due to a decrease in $\Delta\sigma_{LJ}$, while $\Delta\sigma_b$ is relatively constant. The covalent bonds do not contribute directly to the compressive yield stress, but the increased degree of chain

21
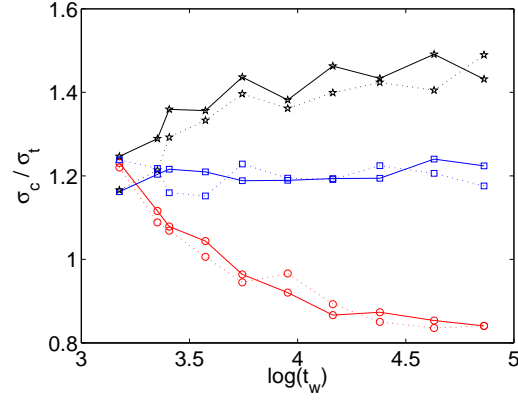
Figure 2.5: Ratio of compressive and tensile yield stress for the unstressed polymer ($\square$) and polymer with pre-stress $\sigma_0 = 0.5$ in the z($\circ$) and x($\star$) direction. Data shown for chains of length $N = 30$ (solid) and $N = 100$ (dotted).

alignment indirectly reduces the LJ stress contribution, since oriented chains can glide more easily past each other (see below).

Fig. 2.4(b) shows the same data set for tensile/compressive yielding in the x-direction perpendicular to the pre-stress. The trends here track those of Fig. 2.4(a) in that compressive strain in the $x$-direction exhibits similar yielding behavior as tensile strain in the $z$ direction. Similarly, tensile strain in the x-direction reduces the yield stress, albeit by a smaller amount than compressive strain in the z-direction. Both tensile and compressive yield are now dominated by frictional stresses from the LJ contributions, since the covalent bonds are not stretched. Data for two different chain lengths $N = 30$ and $N = 100$ are within statistical variation, demonstrating that chain length is not an important factor.

Due to the pressure dependence of shear yielding in glassy polymers [18], the yield stress $\sigma_c$ under compression always exceeds the yield stress $\sigma_t$ under tension even in the absence of any pre-stress. Fig. 2.5 shows the ratio $\sigma_c/\sigma_t$ as a function of $\log(t_w)$ for a system with no pre-stress as well as a system with pre-stress $\sigma_0 = 0.5$ that was subsequently strained in the $z$-and $x$-directions, respectively. For the system with no pre-stress, the ratio $\sigma_c/\sigma_t \approx 1.2$ remains constant with waiting time as $f_b$ remains constant over time (Fig. 2.3). For the system with pre-stress $\sigma_0 = 0.5$, $\sigma_c/\sigma_t$ increases linearly with $\log(t_w)$ for tensile deformation in the z-direction, but decreases when strained in the x-direction. This enhancement or reduction of the tensile/compressive asymmetry is reminiscent of the well-known Bauschinger effect

22

in metals [22] and arises here from the combined effects of increased intrachain tension carried by oriented covalent bonds and a concomitant decrease in interchain friction.

To show that the orientation of the covalent bonds is the main cause for the change in yielding behavior of polymer glasses aged under stress, we repeated the same aging/deformation protocol with a binary (monovalent) Lennard-Jones glass [23] (containing no covalent bonds). The secondary LJ bonds also reorient during aging following the trends of the covalent bonds in the polymer glass, but the value of the orientational order parameter is an order of magnitude less than $f_b$. The dramatic enhancement of the yield stress for uniaxial tension along z or and compression along x is entirely absent. For compression along z and tension along x we observed fluctuations comparable in size to $\Delta\sigma_{yield}$, but no systematic trend.

Our calculations reveal that the history-dependent yielding behavior of aging polymer glasses under applied load results from a complicated interplay between covalent and van der Waals (LJ) forces. While simple aging without pre-stress increases the yield stress due to strengthening of LJ bonds, we show clearly that the origin of any further de- or increase lies in covalent bond alignment. The orientational order parameter $f_b$ changes linearly with respect to $\log(t_w)$ and strain, directly influences the yield stress and causes a Bauschinger effect. These predictions could be verified directly in experiments. Analogous simulations protocols conducted on a binary LJ glass with no covalent bonds show very little change in the yield behavior between different applied pre-stresses, further supporting the conclusion that covalent bond reorientation is responsible for the enhanced yield stress observed in recent experiments [7]. The effect is therefore unique to polymer glasses and is not due to overaging in terms of an accelerated descent on the glassy energy landscape, which has been invoked to explain the effect of deformation on the state of amorphous solids [9, 10]. Such an effect might still be important in the absence of physical aging (e.g. at ultralow temperatures), when mechanical stimulus becomes the only way to induce structural changes.

# References

[1] R. N. Haward and R. J. Young. *The Physics of Glassy Polymers*. Chapman & Hall, London, 1997.

[2] I. M. Ward. *Mechanical Properties of Solid Polymers*. John Wiley & Sons, 1983.

[3] L. C. E. Struik. *Physical aging in amorphous polymers and other materials*. Elsevier/North Holland, 1978.

[4] O. A. Hasan, M. C. Boyce, X. S. Li, and S. Berko. An investigation of the yield and postyield behavior and corresponding structure of poly(methyl methacrylate. *J. Poly. Sc. Part B: Polym. Physics*, 31:185, 1993.

[5] A. L. Volynskii, A. V. Efimov, and N. F. Bakeev. Structural aspects of physical aging of polymer glasses. *Polymer Science Series C*, 49:301, 2007.

[6] J. Rottler and M. O. Robbins. Universal description of aging and rate effects in yield of glassy solids. *Phys. Rev. Lett.*, 95:225504, 2005.

[7] E. T. J. Klompen, T. A. P. Engels, L. E. Govaert, and H. E. H. Meijer. Modeling of the postyield response of glassy polymers: influence of thermomechanical history. *Macromolecules*, 38:6997, 2005.

[8] L. E. Govaert, H. G. H. van Melick, and H. E. H. Meijer. Temporary toughening of polystyrene through mechanical pre-conditioning. *Polymer*, 42:1271, 2001.

[9] D. J. Lacks and M. J. Osborne. Energy landscape picture of overaging and rejuvenation in a sheared glass. *Phys. Rev. Lett.*, 93:255501, 2004.

[10] A. V. Lyulin and M. A. J. Michels. Time scales and mechanisms of relaxation in the energy landscape of deformed polymer glasse: Direct atomictic modelling. *Phys. Rev. Lett.*, 99:085504, 2007.

[11] P. I. Vincent. The necking and cold-drawing of rigid plastics. *Polymer*, 1:7, 1960.

[12] E. J. Kramer. Stress aging in anhydrous nylon 6-10. *J. Appl. Phys.*, 41:4327, 1970.

[13] L. C. E. Struik. The mechanical enhancement of physical aging. *Polymer*, 21:962, 1980.

[14] J. Baschnagel and F. Varnik. Computer simulation of supercooled polymer melts in the bulk and in confined geometry. *J. Phys.: Condens. Matter*, 17:R851, 2005.

[15] R. S. Hoy and M. O. Robbins. Strain hardening of polymer glasses: Effect of entanglement density, temperature, and rate. *J. Polym. Sci. Part B: Polymer Physics*, 44:3487, 2006.

[16] J. M. Hutchinson. Physical aging of polymers. *Prog. Polym. Sci.*, 20:703–760, 1978.

[17] I. M. Ward. *Structure and Properties of Oriented Polymers*. Chapman & Hall, London, 1997.

[18] I. M. Ward. Review: the yield behavior of polymers. *J. Mater. Sci*, 6:1397, 1971.

[19] R. M. Caddell, R. S. Raghava, and A. G. Atkins. A yield criterion for anisotropic and pressure dependent solids such as oriented polymers. *J. Mater. Sci*, 8:1641, 1973.

[20] M. D. Shelby and G. L. Wilkes. The effect of molecular orientation on the physical ageing of amorphous polymers - dilatometric and mechanical creep behavior. *Polymer*, 39:6767, 1998.

[21] A. De. Francesco and R. A. Duckett. Effects of orientation on mechanical properties of unizxially oriented polystyrene films. *Polymer*, 45:8005, 2004.

[22] J. Bauschinger. Ueber die Veränderung der Elasticitätsgrenze und des Elasticitätamoduls Verschiedener Metalle. *Zivilingenieur*, 27:289–348, 1881.

[23] W. Kob and H. C. Andersen. Testing mode-coupling theory for a supercooled binary Lennard-Jones mixture i: The van Hove correlation function. *Phys. Rev. E*, 51:4626, 1995.

# Chapter 3

# Physical Aging and Structural Relaxation in Polymer Nanocomposites [1]

## 3.1 Introduction

The technique of adding nanoscopic fillers to polymeric materials has drawn significant interest in the last two decades as it provides the prospect of developing materials with new and improved properties [1–4]. The popularity of nanoparticles over micrometer-sized filler is due to the large surface area to volume ratio, requiring only small concentrations of fillers to result in significant changes in the polymer matrix [5]. In order to control and design the properties of polymer nanocomposites (PNC), a detailed understanding of the physics and chemistry at the polymer-nanoparticle interface is needed [1, 5]. Experiments show that the glass transition temperature $T_g$, stability and mechanical properties are a complex function of filler concentration, dispersion and interfacial interactions [5–7]. Unfortunately, the properties of the interfacial region are very difficult to measure, and its structure and physics remain difficult to characterize. An additional complication arises from the presence of physical aging, which leads to a slow evolution of an amorphous material towards its thermodynamic equilibrium.

All polymer glasses undergo physical aging [8], and almost all of their physical properties change as a result. Aging can have a detrimental effect on the fracture toughness, as it promotes the tendency for strain localization. Therefore, understanding and controlling the effect of aging on mechanical properties is essential for predicting the lifetime to failure, and critical to the design of polymeric materials.

[1]A version of this chapter has been published. Liu, A. Y.- H and Rottler, J. (2009) Physical Aging and Structural Relaxatino in Polymer Nanocomposites, *Journal of Polymer Science: Part B: Polymer Physics* Vol 47, 1789-1798.

Aging can manifest itself in two distinct ways [8, 9]: First, due to slow structural relaxations, thermodynamic variables such as density, internal energy and enthalpy change logarithmically with the waiting time $t_w$ elapsed since the glass was formed. In contrast, structural (alpha-) relaxation times increase as a power law, $\tau_\alpha \sim t_w^\mu$, where $\mu$ is called the aging exponent. $\mu$ can be deduced by measuring dynamical variables such as the creep response under constant load, and then shifting the resulting creep compliance curves for different $t_w$ onto one master curve [8].

There is an extensive literature on the effect of confinement on $T_g$ in thin polymer films [6, 10–13]. Simulation studies of supercooled polymer films have also investigated the dynamics as a function of film thickness [14–17]. Some experimental results indicate that polymer nanocomposites also exhibit different $T_g$ values than a neat polymer [18]. Much less work, however, has been devoted to the effect of confinement on the out-of-equilibrium dynamics in the aging regime [19, 20], none of which explores both manifestations of aging simultaneously.

In the present work, we use molecular dynamics simulations to investigate physical aging in simple model polymer composite systems. Our goal here is not to quantitatively reproduce specific experimental systems, but rather to explore generic scenarios and measure microscopic quantities which are not easily accessible in experiments. We shall consider a coarse-grained polymer model and idealized, spherical nanoinclusions at several concentrations with different interfacial properties. Modeling on this level does not include chemical detail, but permits a greater flexibility in length and time scales. Similar models were employed in the past to examine the inclusion of nanoparticles in polymer melts [21, 22] and glasses [23–25]. For instance, ref. [23] studied the impact on the glass transition temperature from a single polygonic nanoparticle (with force sites on the surface) immersed in a polymer matrix. There are experimental results where a reduction of the physical aging rate was reported for systems with attractive polymer-nanoparticle interactions [18, 26]. There are also limited results on the creep compliance of nanocomposites, which reported no significant changes in the mechanical shift factors and hence the aging exponents due to the presence of nanoinclusions [27]. This suggests that the two manifestations of aging, while both used extensively as a way to evaluate the aging behavior, may be affected differently in confined systems. In our simulations, we simultaneously monitor the confinement effect of the nanospheres on the evolution of macroscopic thermodynamic properties (energy, density) as well as the change in structural relaxation times via microscopic
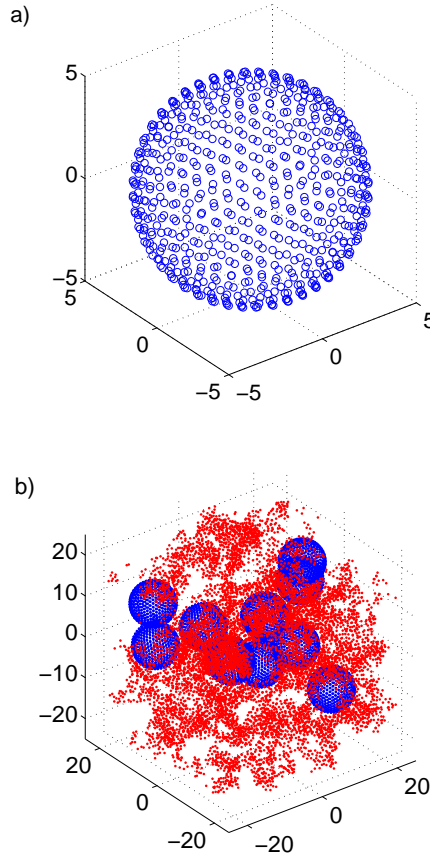
Figure 3.1: a) Example of a nanoparticle with interaction sites.  b) Snap shot of a simulation of a PNC system with 10 nanoparticles and polymer chains (not all polymer chains are shown).

dynamics. In particular, we will isolate the interface from bulk behavior to distinctly characterize the interfacial region.

## 3.2  Model Systems

Molecular dynamics is used to simulate a bead-spring polymer system, which has been used extensively in studies of glassy dynamics [14, 28, 29]. The beads are bonded via a finite extensible nonlinear elastic (FENE) spring, and van der Waals forces between the beads are modeled with a truncated 6-12 Lennard Jones (LJ) potential:

$$V_{\text{LJ}}(r) = 4\epsilon \left[ \left( \frac{\sigma}{r} \right)^{12} - \left( \frac{\sigma}{r} \right)^{6} \right] \qquad \text{for } r < r_c \qquad (3.1)$$

The parameters of the LJ potential $\sigma$ and $\epsilon$ are used as reference length and energy scales respectively. The reference time scale is $\tau_{LJ} = \sqrt{m\sigma^2/\epsilon}$. All results are given in these units unless otherwise stated. We consider 810 chains of 100 beads each in a cubic box subject to periodic boundary conditions. For the simulations described in this paper, 10 or 20 "nanoparticle spheres" corresponding to 6 and 12 percent volume fraction were added to this neat system to study the effect of fillers. Each nanoparticle is a rigid sphere of diameter 10, whose surface is covered with about 640 LJ beads (interaction sites) on the vertices resulting from the tessellation of the sphere's surface, see Fig. 3.1(a).

The parameters $\epsilon$ and $r_c$ were varied to tune the polymer-polymer and polymer-nanofiller interactions. For polymer-polymer interactions we always use $\epsilon = 1$, $r_c = 1.5$. We also consider two kinds of nanospheres with the representative parameters $\epsilon = 1$, $r_c = 1.1225$ to model a purely repulsive, nonwetting sphere and $\epsilon = 2.5$, $r_c = 2.5$ for a strongly attractive sphere. Pair correlation functions $g(r)$ for the resultant systems in the glassy state for both types of interactions are shown in Fig. 3.2. Here $g(r)$ is computed between the polymer atoms and the center of the nanospheres. One can see that for the PNC system with attractive polymer-nanoparticle interactions $g(r)$ has high peaks near the surface of each nanosphere (beginning at $r = 6$, which is the distance between the center of a nanosphere and the center of a polymer atom directly attached to its surface). For the repulsive case $g(r)$ is essentially flat.

To make the glass, the PNC system is initialized using a random walk process, then a cosine push-off potential is used to ensure separation between all the polymer atoms and nanoparticle spheres before the interchain LJ interaction is applied. After equilibrating this system at $T = 1.2$ at zero pressure, a rapid quench takes the system to $T = 0.2$ under constant pressure. The temperature during the quench is controlled using a Langevin thermostat. The change in volume as a function of temperature during the quench is shown in Fig. 3.3 for three different systems: neat polymer, and PNC with attractive and repulsive nanospheres. The curves exhibit the shape of a typical glass-transition, and the change in slope between the high temperature and low temperature region can be used to define a glass transition temperature. One can see that a so-defined $T_g$ is slightly higher for attractive interactions and lower for repulsive interactions with respect to the neat system. This is consistent with trends
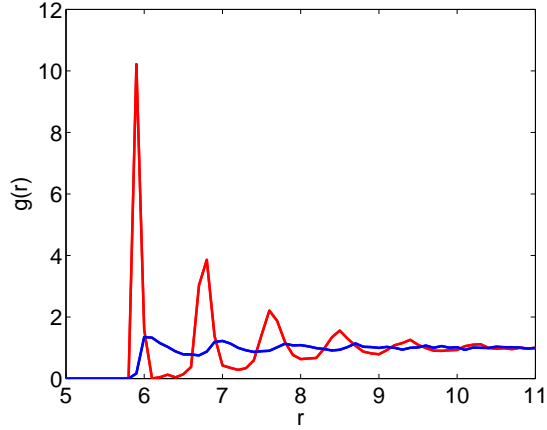
Figure 3.2: Pair-correlation function showing the difference in structure between repulsive (blue) and attractive (red) nanoparticles.

found in experiments [18] and previous simulations [23], but we note that fitting the terminal slopes involves considerable uncertainties.

After the polymer-glass is formed, it is aged in both constant pressure-temperature (NPT) and constant volume-temperature (NVT) ensembles for a waiting time $t_w$ via Nose-Hoover thermostats/barostats. The mean-squared displacement, creep compliance and thermodynamical variables such as energy are then measured for times $t$ and different wait times $t_w$.

## 3.3 Results

### 3.3.1 Aging in the Neat Polymer Glass

We begin by characterizing the aging process in the neat polymer without nanospheres. As discussed in ref. [30], a convenient way to monitor relaxation on a microscopic level is to compute the mean squared displacement of all beads,

$$\langle \Delta \mathbf{r}(t, t_w)^2 \rangle = \frac{1}{N} \sum_{j=1}^{N} \left( \mathbf{r}_j(t) - \mathbf{r}_j(t_w) \right)^2 . \tag{3.2}$$

The resulting curves (see Fig. 3.4) show distinct regions of ballistic, caged and cage-escape behavior, and the cage escape time increases with $t_w$. The inset of Fig. 3.5 shows that the aging part of the curves (where departure from the cage plateau begins
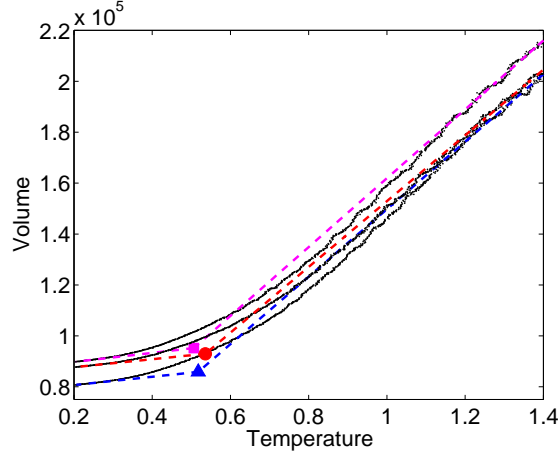
Figure 3.3: Cooling curves for three different systems: neat (▲) polymer, repulsive (■), and attractive (●) PNC at 6 Vol%. Linear extrapolation of the high and low temperature slopes defines a glass transition temperature.

to take place) can be superimposed along the time axis with shift factors $a$ to collapse onto one master curve. The shift factors obey a power law relation $a \sim t_w^{-\mu}$ (see Fig. 3.5), which is characteristic of aging. As mentioned previously, $\mu$ is called the aging exponent and describes the increase of structural relaxation times with respect to $t_w$. For many polymer glasses $\mu$ is close to one near $T_g$, decreases with decreasing temperature, and vanishes for temperatures above $T_g$[9].

In addition to the slowing down of the dynamics, bulk thermodynamic variables also change during aging. As an example, Fig. 3.6 shows that the LJ potential energy per polymer bead changes logarithmically with aging time, as expected from the classic macroscopic response during physical aging [9]. Similar curves are found for volume relaxation. The macroscopic physical aging rate may be conveniently defined as the logarithmic slope

$$r_e = \frac{1}{E_0}\frac{dE}{d\log(t)} \quad , \quad r_v = -\frac{1}{V_0}\frac{dV}{d\log(t)}, \tag{3.3}$$

which can be extracted through linear fits to the data in Fig. 3.6. The physical aging rate is higher in the NPT ensemble due to the additional contribution from constant pressure, but not qualitatively different. All results discussed in the following were obtained in the NVT ensemble.
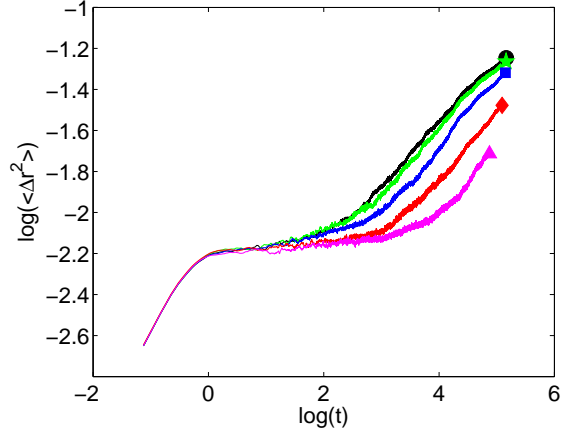
Figure 3.4: Mean-squared displacements for the neat system at various waiting times: $t_w = 1500$ (●), $t_w = 2250$ (⋆), $t_w = 5550$ (■), $t_w = 24000$ (♦) and $t_w = 72750$ (▲).
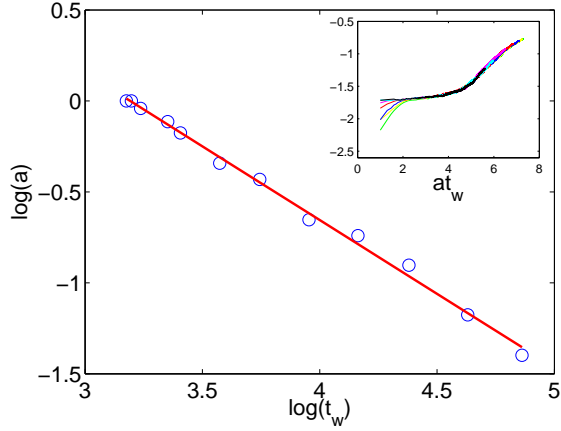


Figure 3.5: Shift factor $a$ versus $t_w$ for the neat system. Straight line is a power law fit with slope $\mu = 0.81$. The inset shows $\langle \Delta \mathbf{r}^2 \rangle$-curves from Fig. 3.4 rescaled by a shift factor $a$ to superimpose on the oldest curve.
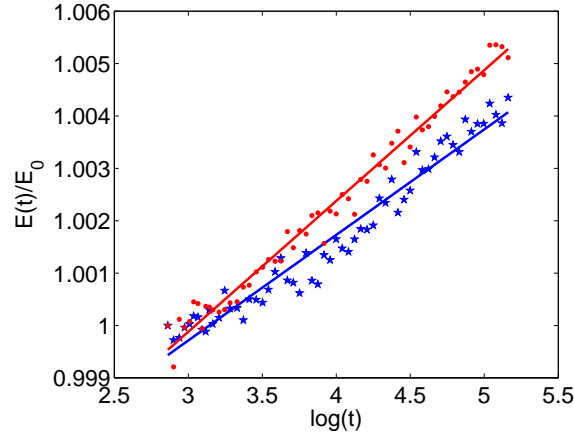
Figure 3.6: Relaxation of the LJ energy per bead as a function of aging time in both NVT ($\star$) and NPT ($\bullet$) ensembles. Logarithmic slopes define the physical aging rate $r_e$ (see text).

## 3.3.2 Aging in Nanocomposites

In this section, we explore how the aging behavior of the neat polymer is modified by the addition of attractive or repulsive nanospheres at two different concentrations as described in Section II.

### 3.3.2.1 Aging of structural relaxation times

In order to determine changes in the global structural relaxation time of the polymer glass, we measured again the mean squared displacement using the same procedures as discussed before for the neat system. The resulting $\langle \Delta \mathbf{r}^2 \rangle$-curves were also found to obey time-aging superposition and can be superimposed onto one single master curve by shifting along the time axis with shift factors $a$. Corresponding aging exponents $\mu$ were determined in the same manner by fitting to the power law $a \sim t_w^{-\mu}$ (see below).

Since the effect of nanofillers is expected to be strongest at the polymer-filler-interface, we now separately analyze particle diffusion in the interfacial and bulk regions. The interfacial regions are defined as spherical shells of thickness $1.5\sigma$ and $2.5\sigma$ surrounding each nanoparticle. These shells include the first and second peak of the pair correlation function, as shown in Fig. 3.2. For the system with attractive polymer-nanoparticle interactions (Fig. 3.7(a)), three sets of curves are shown. First, diffusion in the bulk region is fastest and almost identical to the neat system (see
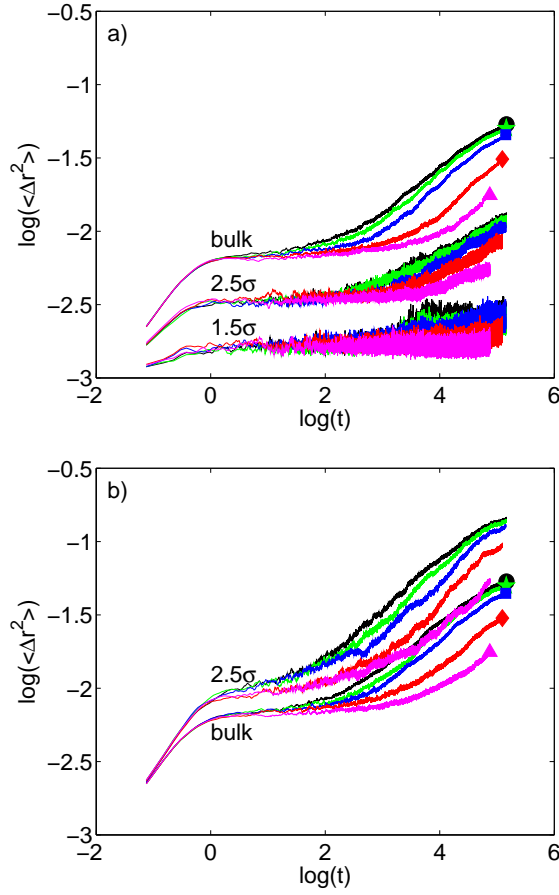
Figure 3.7: a) $\langle \Delta \mathbf{r}^2 \rangle$ for a PNC system with attractive polymer-nanoparticle inter-actions. $1.5\sigma$ and $2.5\sigma$ interfacial as well as bulk region shown separately. b) $\langle \Delta \mathbf{r}^2 \rangle$ for a repulsive system in a $2.5\sigma$ interfacial as well as bulk region. Waiting times as in Fig. 3.4

Fig. 3.4). The sets of curves below correspond to the $2.5\sigma$ and $1.5\sigma$ interfacial regions and show that the mobility is much reduced in the vicinity of the nanoparticle, with the reduction being more dramatic in the $1.5\sigma$ region where all polymer beads touch the surface of the nanospheres. For the system with repulsive polymer-nanoparticle interactions (Fig. 3.7(b)), $\langle \Delta \mathbf{r}^2 \rangle$-curves for the bulk and $2.5\sigma$ interfacial regions are shown. The bulk region exhibits $\langle \Delta \mathbf{r}^2 \rangle$-curves that are essentially identical to those for the bulk region of a system with attractive interactions, as well as those from the neat system. Strong deviations from bulk behavior occur only near the interface, where now the motion of beads is accelerated and diffusion is faster. In the present
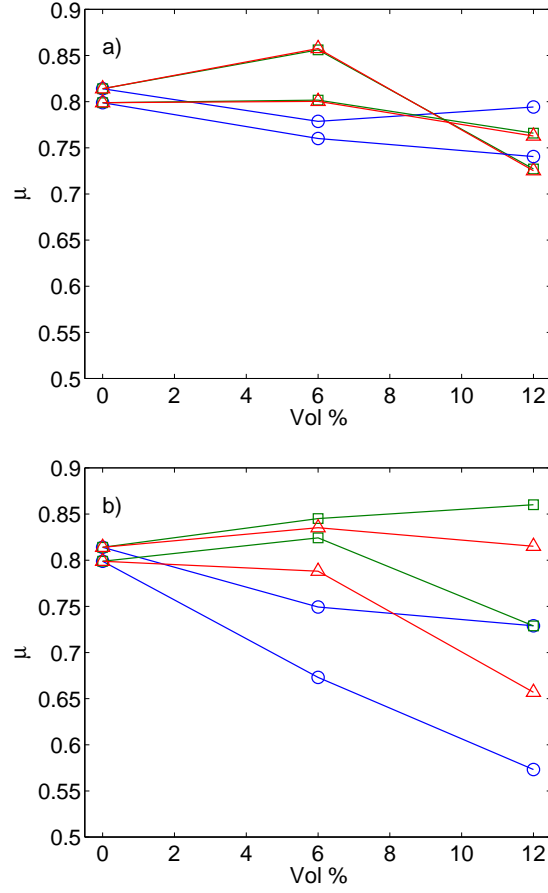
Figure 3.8: Summary of aging exponents $\mu$ ($\triangle$) , $\mu_{bulk}$ ($2.5\sigma$-region, $\square$) and $\mu_{int}$ ($\circ$) for two independent PNC samples with attractive a) and repulsive b) polymer-nanoparticle interactions. (Data for the two independent samples have the same symbols and are connected by lines.)

simple PNC model with coarse-grained polymer chains, the effect on the microscopic dynamics due to the presence of nanospheres is only observed in the interfacial region between the polymer matrix and the nanoparticles. Similar trends were found previously in a simulation of a PNC in the melt [22].

Interestingly, despite the contrasting diffusion behavior between the interfacial and bulk regions, the relative change in relaxation times for different $t_w$ (or shift factor $a$) does not appear to differ much between the interfacial and bulk regions. For the attractive case, curves in the $2.5\sigma$ region appear to undergo almost the same shift with aging time as in the bulk region (in the $1.5\sigma$ region the dynamical range

is too small for a definitive conclusion). Similarly, shifts in the $1.5\sigma$ repulsive region also appear unaffected.

To quantify this behavior, we measured separately aging exponents $\mu_{bulk}$ and $\mu_{int}$ ($2.5\sigma$-region) from superposition of the corresponding $\langle\Delta\mathbf{r}^2\rangle$-curves. Results are summarized in Fig. 3.8 as a function of concentration for two independent sets of samples to indicate variability. Here we also show results for the aging exponent $\mu$ obtained in the entire system. For the attractive spheres, the aging exponent $\mu_{int}$ varies only in a narrow band between 0.72-0.85 for all regions and concentrations. For the repulsive spheres, the spread is somewhat bigger and $\mu_{int}$ appears to be slightly reduced near the interface, but the trend is weak within uncertainties. Although the cage escape time is enhanced or reduced in absolute terms, the relative shifts are not affected unless particles are completely immobilized. These generic trends are consistent with those of ref. [27], in which the creep compliance of Polyamide 6 nanocomposites with different types and concentrations of layered silicate particles (with attractive polymer-silicate interactions due to the presence of hydrogen bonds) were measured. The study reported aging exponents to be in the same range as the unfilled polymer systems.

### 3.3.2.2 Physical aging rate

In addition to the microscopic dynamics, we also determined the physical aging rate $r_e$ (eq. (3.3)) in nanocomposite systems. We computed the average pair energy per polymer particle separately within the interfacial region of size $2.5\sigma$ and the remaining bulk region in Fig. 3.9; the logarithmic slope of the curves yields $r_e$. Pairwise interactions across the dividing surface are attributed equally to both regions. In both attractive and repulsive systems, the physical aging rates in the bulk ($\square$ and $\circ$ for 6 and 12 Vol%, resp.) are very similar and almost unchanged from those observed in the neat system (solid line). They also do not seem to be dependent on concentration. In agreement with the findings for particle mobility, $r_e$ is affected by the nanoparticles only in the interfacial regions, where it is reduced for attractive and increased for repulsive nanospheres ($\star$ and $\triangle$ for 6 and 12 Vol%, resp.). Values for $r_e$ relative to the value in the neat system are summarized in Figs. 3.10(a) and 3.11(a).

Since the physical aging rate appears to behave in a similar manner to the magnitude of the mean squared displacement, it is interesting to ask if there is a more quantitative relationship. To this end, we define a measure of mobility $m$ as the value
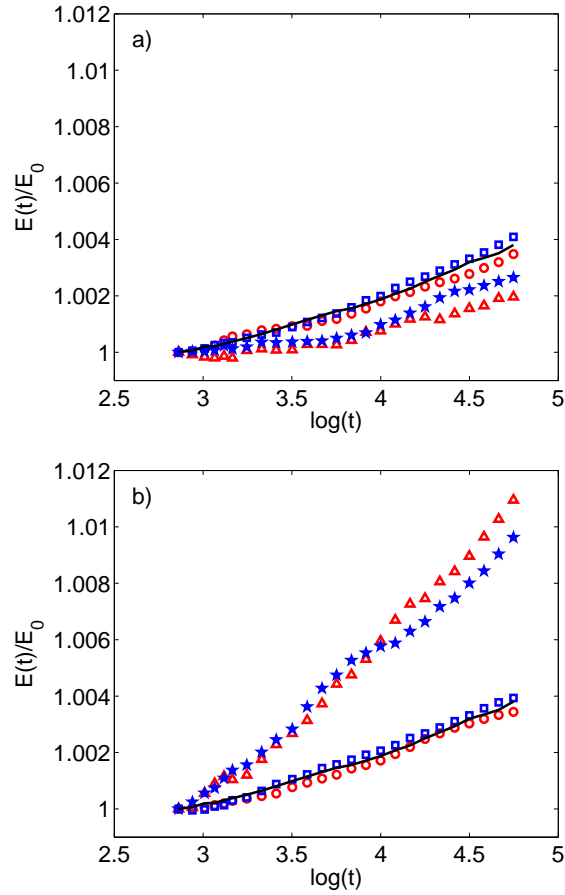
Figure 3.9: a) Energy relaxation of PNC systems with attractive polymer-nanoparticle interaction at two different concentrations in the interfacial regions for 6 Vol% ($\star$) and 12 Vol% ($\triangle$), and bulk for 6 Vol% ($\square$) and 12 Vol% ($\circ$). b) Same data for a PNC system with repulsive polymer-nanoparticle interactions.
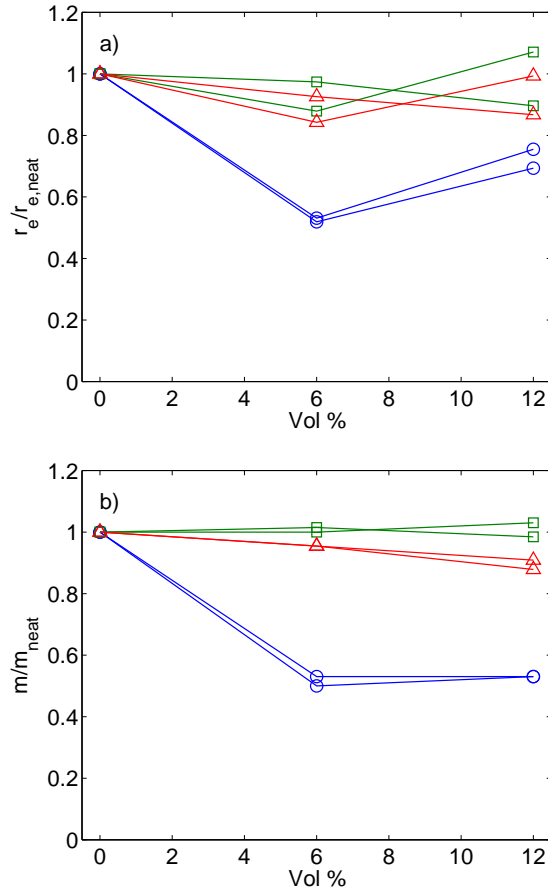
Figure 3.10: (a) Physical aging rates $r_e$ of the attractive system relative to the rate $r_{e,neat}$ for the neat system in the $2.5\sigma$ interfacial ($\circ$), bulk ($\square$) and total ($\triangle$) regions. (b) Mobility $m$ (see text) relative to the neat system in the same regions as in (a). As in Fig. 3.8, data for two independent PNC samples are shown with the same symbols.
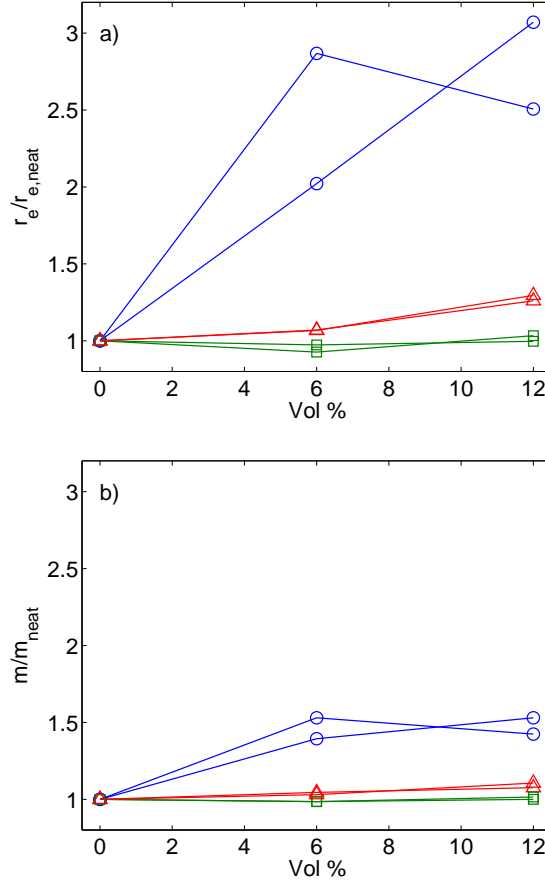
Figure 3.11: (a) Relative physical aging rates (a) and mobilities (b) for the repulsive system. Symbols as in Fig. 3.10.

of $\langle \Delta \mathbf{r}^2 \rangle$ at the cage plateau and plot this quantity normalized by the values for the neat system in Figs. 3.10(b) and 3.11(b) for direct comparison with the $r_e$-values. For the attractive case, we see that the relative mobility very closely tracks the relative $r_e$ values, with both being reduced by about 50% near the interface. For the repulsive system, both quantities are enhanced relative to the bulk value, but the quantitative agreement is less clear.

### 3.3.2.3 Size of Interfacial Region

Even though aging in the interfacial regions is affected non-trivially by presence of nanoinclusions, the bulk behavior does not deviate significantly from that in the neat polymer glass. In order to gain further insight into the range over which the

nanoparticles affect the polymer matrix, we systematically increase the size of the interfacial region from 1.5 to $8\sigma$ and track both $r_e$ and $m$ as a function of width of the interface. In Fig. 3.12(a) showing data for the attractive system, it can be seen that $r_e$ is smallest immediately near the interface, but reaches the value measured for the total system once the interfacial region increases to about $6\sigma$. The mobility varies over the same range. For the repulsive system the trends are reversed, and saturation to the total values occurs earlier around $4\sigma$. In the present polymer model, the effects of the nanoparticles are therefore limited to distances much smaller than the average distance between nanoparticles, which is about $10\sigma$ to $12\sigma$ for the volume fractions studied here. This is consistent with the lack of confinement effects in the bulk regions, and the absence of a stronger deviation from the total aging behavior as seen in experimental systems [18, 26].

#### 3.3.2.4  Creep compliance

In experiments, shift factors are usually determined by measurements of the creep compliance $J(t, t_w)$. Ref. [30] showed that mechanical shift factors obtained from superimposing compliance curves at different waiting times track those obtained from mobility (mean squared displacement) measurements for different applied stresses. To complete the characterization of the PNC systems, we show a representative set of compliance curves in Fig. 3.13 for a neat system as well as attractive and repulsive PNC system. The compliance was determined by applying a uniaxial tensile stress in one direction, while maintaining zero stress in the perpendicular directions, and measuring the resulting engineering strain. In all three systems, compliance curves shift to longer times with increasing $t_w$ and obey time-waiting time superposition. In general, the attractive system is less compliant and the repulsive system more compliant than the neat polymer. However, shift factors are mostly unaffected and vary little between the three systems. The aging exponents $\mu_J$ determined from the mechanical measurement follow the same trends as the $\mu$ values from diffusion in the total system (see Fig. 3.8). These findings also agree with the results of ref. [27], where the creep compliance of Polyamide 6 was reduced by about a factor of two under the addition of layered silicate (which have attractive interactions via hydrogen bonds). In addition, the shape of the creep curves and the corresponding aging exponents were not altered significantly by the addition of nanoinclusions.
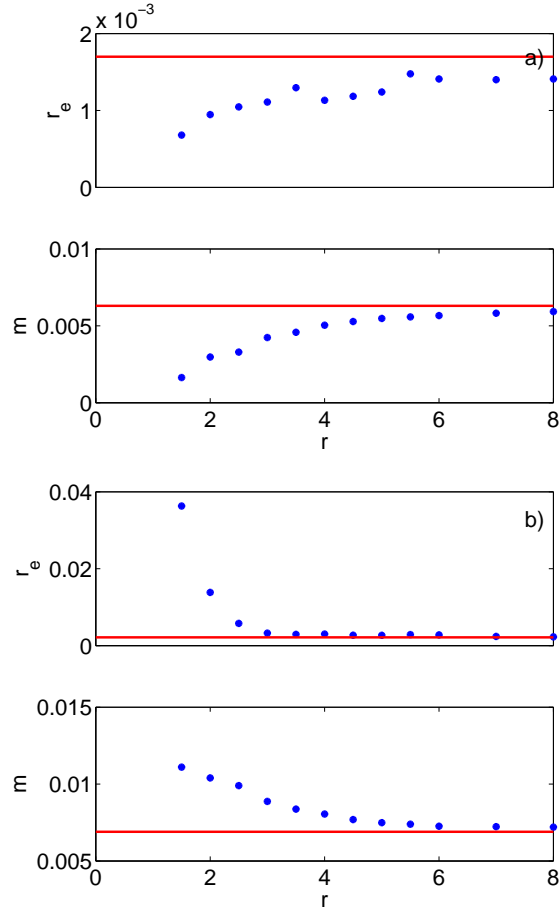
Figure 3.12: Aging rate and mobility as a function of distance from the polymer-nanoparticle interface for a) attractive PNC system and b) repulsive PNC system. Solid red lines indicate the values in the total system.
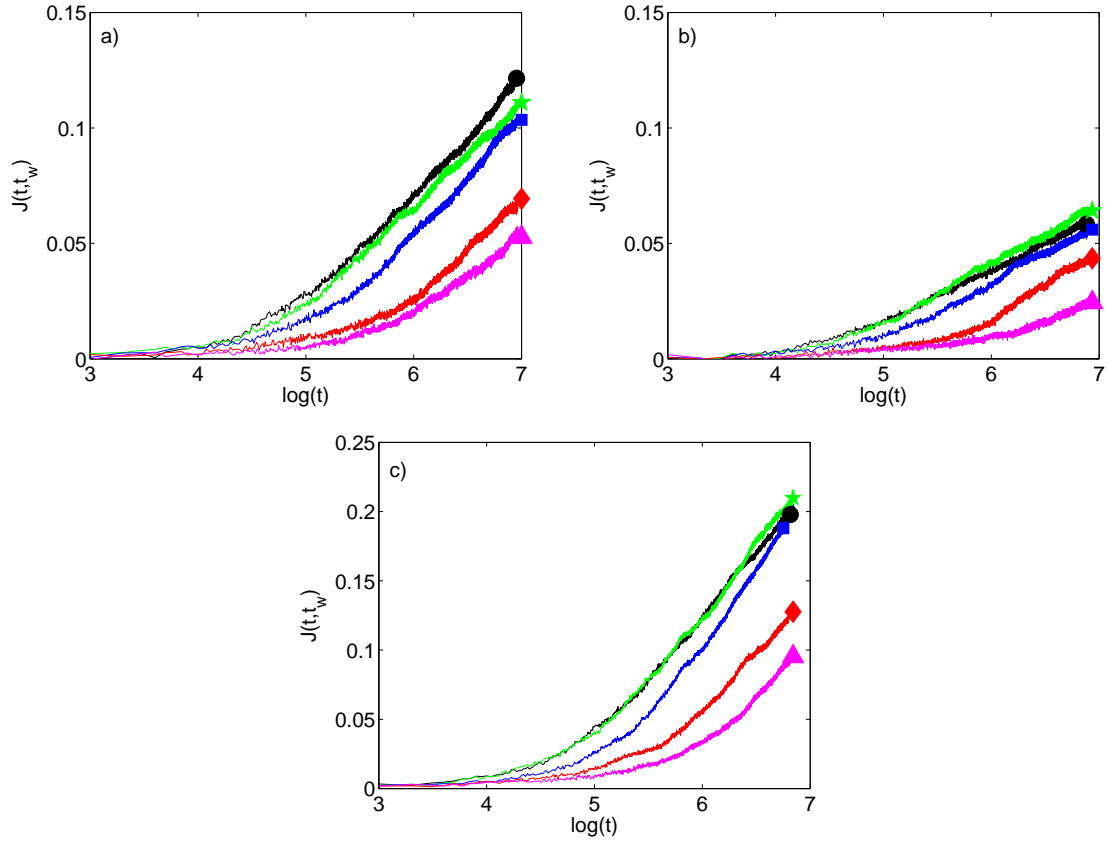
Figure 3.13: Creep compliance $J(t, t_w)$ for uniaxial loading with constant stress of 0.4 for (a) neat system, (b) PNC system with 6 Vol% attractive nanospheres and (c) PNC system with 6 Vol% repulsive nanospheres. Aging exponents resulting from superposition of these curves are $\mu_J = 0.79, 0.76, 0.69$. Waiting times as in Fig. 3.4.

## 3.4   Discussion

Using a model PNC system with bead-spring polymer chains and spherical nanoinclusions with attractive and repulsive Lennard-Jones interactions, it was found that there are substantial differences between the effect of nanoparticles seen in the interfacial and bulk regions. In the interfacial regions, we found that the aging behavior of the polymeric system is dramatically altered by the addition of nanospheres. The physical aging rate as measured through changes in the pair energy per particle is reduced near the attractive polymer-nanosphere interface. The mobility $m$, which is a measure of the structural relaxation time, decreases by about the same amount. This supports the idea that near the attractive nanosphere, there is suppression of motion (hence the lower $m$) that is associated with structural relaxations, which in turn cause the suppression of $r_e$, as suggested by eg. ref. [19]. The same idea is also consistent with the repulsive polymer-nanosphere interfaces, where $r_e$ and $m$ are both enhanced significantly compared to their bulk values.

   Although the structural relaxation time is modified in absolute terms, shift factors and resulting aging exponents found from the mean-squared displacement in the same systems do not change measurably between the interfacial and bulk regions. They also do not exhibit the trends seen for the physical aging rate and mobility with respect to the different types of polymer-nanoparticle interactions. In fact, the slight decrease of $\mu_{\mathrm{int}}$ found for the repulsive spheres contrasts the increase in physical aging rate. Similarly, while the magnitude of the creep compliance is reduced by the addition of nanoparticles with attractive polymer-nanoparticle interactions, relative mechanical shift factors and aging exponents do not deviate significantly from the neat system. If a power law form $\tau_\alpha \sim t_w^\mu$ for the behavior of the structural relaxation time is assumed, the present results suggest that confinement primarily affects the prefactor, but not the exponent. It is important to realize, however, that physical aging rate and aging exponent describe different aspects of aging. The aging exponent is primarily a measure of the memory of the system, while the physical aging rate is related to the absolute change of material properties. Since the aging exponent controls the growth of the primary structural relaxation rate, our results indicate that its relationship to the physical aging rate is more complicated.

   We also characterized the size of the region exhibiting modulated aging behavior by tracking $r_e$ and $m$ as a function of distance from the polymer-nanosphere interface and found it to be much smaller than the average distance between the nanoparti-

cles. This is consistent with the fact that for our model system, the net effect of confinement on the total aging behavior is weak and the model cannot reproduce the large stability increase seen in some experiments such as ref. [18]. This indicates that in real polymers some nonlocal effects must contribute to the stabilization of the polymer matrix that are not represented in the model system used in this work. One possible approach to better represent real polymer systems might involve increasing the complexity of the model to include details such as chemical specificity and more details on the polymer-nanosphere interface.

The main findings in this work lead to the notion that the two manifestations of aging may be affected differently by the presence of nanoinclusions. Experimental studies of nanocomposites have so far only focused either on the physical aging rate, or on the mechanical behavior and the resulting shift behavior. The present study shows that a better understanding of the relationship between aging exponents and aging rate would be a fruitful topic for further research.

## 3.5 Acknowledgements

# References

[1] F. Hussain, M. Hojjati, M. Okamoto, and R. Gorga. Polymer-matrix nanocomposites, processing, manufacturing and application: an overview. *J. Composite Mat.*, 40:1511, 2006.

[2] D. Blond, V. Barron, M. Ruether, K. Ryan, V. Nicolosi, W. Blau, and J. Coleman. Enhancement of modulus, strength and toughness in poly(methyl methacrylate)-based composites by the incorporation of poly(methyl methacrylate)-functionalized nanotubes. *Advanced Functional Materials*, 16:1608, 2006.

[3] J. Coleman, M. Cadek, K. Ryan, A. Fonseca, J. Nagy, W. Blau, and M. Ferreira. Reinforcement of polymers with carbon nanotubes. the role of an ordered polymer interfacial region. experiment and modeling. *Polymer*, 47:8556, 2006.

[4] B. Ash, R. Siegel, and L. Schadler. Mechanical behavior of alumina/poly(methyl methacrylate) nanocomposites. *Macromolecules*, 37:1358, 2004.

[5] L. Schadler, L. Brinson, and W. Sawyer. Polymer nanocomposites: a small part of the story. *JOM*, 59:2007, 2007.

[6] C. Ellison and J. M. Torkelson. The distribution of glass-transition temperatures in nanoscopically confined glass formers. *Nature Materials*, 10:695, 2003.

[7] T. Ramanathan, H. Liu, and L. C. Brinson. Functionalized swnt/polymer nanocomposites for dramatic property improvement. *J. Poly. Sci.: Part B: Polymer Physics*, 44:470, 2006.

[8] L. C. E. Struik. *Physical aging in amorphous polymers and other materials.* Elsevier, Amsterdam, 1978.

[9] J. M. Hutchinson. Physical aging of polymers. *Prog. Polym. Sci.*, 20:703–760, 1978.

[10] J. Keddie, R. Jones, and R. Cory. Size-dependent depression of the glass transition temperature in polymer films. *Europhys. Lett.*, 27:59, 1994.

[11] J. Forrest and K. Dalnoki-Veress. The glass transition in thin polymer films. *Advances in Colloid and Interface Science*, 94:167, 2001.

[12] M. Alcoutlabi and G. B. McKenna. Effect of confinement on material behavior at the nanometre size scale. *J. Phys.: Condens. Matter*, 17:R461, 2005.

[13] C. Svanberg. Glass transition relaxations in thin suspended polymer films. *Macromolecules*, 40:312, 2007.

[14] J. Baschnagel and F. Varnik. Computer simulation of supercooled polymer melts in the bulk and in confined geometry. *J. Phys.: Condens. Matter*, 17:R851, 2005.

[15] S. Peter, H. Meyer, and J. Baschnagel. Thickness-dependent reduction of the glass transition temperature in thin polymer films with a free surface. *J. Poly. Sci.: Part B: Polymer Physics*, 44:2951, 2006.

[16] A. Baljon, M. Van Weert, R. Degraaff, and R. Khare. Glass transition behavior of polymer films of nanoscopic dimensions. *Macromolecules*, 38:2391, 2005.

[17] J. Torres, P. Nealey, and J. de Pablo. Molecular simulation of ultrathin polymeric films near the glass transition. *Phys. Rev. Lett.*, 85:3221, 2002.

[18] P. Rittigstein and J. M. Torkelson. Polymer-nanoparticle interfacial interactions in polymer nanocomposites: confinement effects on glass transition temperature and suppression of physical aging. *J. Poly. Sci.: Part B: Polymer Physics*, 44:2935, 2006.

[19] R. Priestley, C. Ellison, L. Broadbelt, and J. M. Torkelson. Structural relaxation of polymer glasses at surfaces, interfaces, and in between. *Science*, 309:456, 2005.

[20] R. Priestley. Physical aging of confined glasses. *Soft Matter*, 5:919, 2009.

[21] M. Vacatello. Monte Carlo simulations of polymer melts filled with solid nanoparticles. *Macromolecules*, 34:1946, 2001.

[22] T. Desai, P. Keblinski, and S. Kumar. Molecular dynamics simulations of polymer transport in nanocomposites. *J. Chem. Phys.*, 122:134910, 2005.

[23] F. W. Starr, T. B. Schroder, and S. C. Glotzer. Effects of a nanoscopic filler on the structure and dynamics of a simulated polymer melt and the relationship to ultrathin films. *J. Chem. Phys.*, 64:021802, 2001.

[24] G. J. Papakonstantopoulos, K. Yoshimoto, M. Doxastakis, P. F. Nealey, and J. J. de Pablo. Local mechanical properties of polymeric nanocomposites. *Phys. Rev. E*, 72:031801, 2005.

[25] G. J. Papakonstantopoulos, M. Doxastakis, P. F. Nealey, J.-L. Barrat, and J. J. de Pablo. Caculation of local mechanical properties of filled polymer. *Phys. Rev. E*, 75:031803, 2007.

[26] H. Lu and S. Nutt. Enthalpy relaxation of layered silicate-epoxy nanocomposites. *Macromol. Chem. Phys.*, 204:1832, 2003.

[27] D. P. N. Vlasveld, H. E. N. Bersee, and S. J. Picken. Creep and physical aging behavior of PA6 nanocomposites. *Polymer*, 46:12539, 2005.

[28] K. Kremer and G. S. Grest. Dynamics of entangled linear polymer melts: a molecular dynamics simulation. *J. Chem. Phys*, 92:5057, 1990.

[29] K. Binder (Eds). *Monte Carlo and molecular dynamics simulations in polymer science.* Oxford, 1995.

[30] M. Warren and J. Rottler. Simulations of aging and plastic deformation in polymer glasses. *Phys. Rev. E*, 76:031802, 2007.

# Chapter 4

# Conclusion and Open Questions

By using a simple bead-spring polymer system, we were able to simulate trends found in recent experiments. In polymer glasses, the yield stress increases as a function of waiting time $t_w$. This increase was further enhanced for polymer glasses aged under uniaxial tensile stress $\sigma_0$, effectively "overaging" the system. This enhancement in yield stress was also found to be proportional to $\sigma_0$, consistent with the findings in ref. [1]. By straining the system in a direction perpendicular to the pre-stresses and determining the corresponding yield stress, the opposite trend was found and the rate of increase in yield stress with respect to $t_w$ was suppressed, indicating the presence of orientation effects. To confirm this, we defined an order parameter to characterize the degree of covalent and LJ bond alignment and tracked it over the time in which the system was aged under $\sigma_0$ . It was found that the change in the covalent bond orientation strongly dominates over the LJ bond contributions, and that it increased as a function of logarithmic time. This increase was directly proportional to the enhancement in yield stress for tensile strain in the direction parallel to the pre-stress, and to the suppression in yield stress for tensile strain in the direction perpendicular to the pre-stress.

Although not explicitly stated in chapter 3, we further showed that the amount of strain softening is unaffected by the bond re-orientation, and that the change in yield stress is due to the stretching of covalent bonds. This is demonstrated explicitly in Fig. 4.1, where contributions from the LJ stress and the covalent stress are separated. While little change can be seen in the LJ component (which is subject to aging), the rise in yield stress for the covalent component (which is not subject to aging) is proportional to the strain hardening slope. This further supports the conclusion that apart from an initial transient, the intrinsic aging behavior is not fundamentally altered by the application of stress.

To further demonstrate that the re-orientation of the covalent bonds was responsible for this observed change in yield behavior, we repeated the same experimental protocol using a model binary Lennard-Jones glass. The lack of covalent bonds means
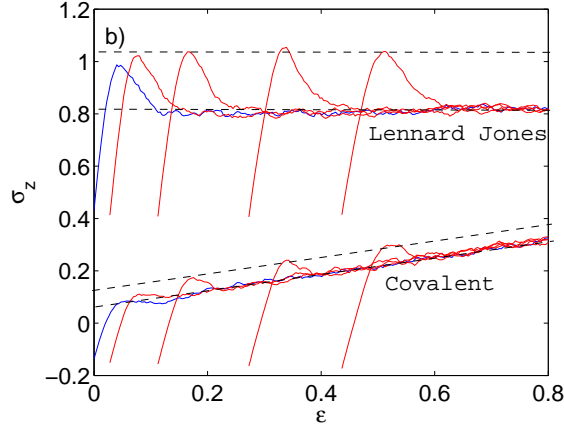
Figure 4.1: Stress-strain curves for $\sigma_0 = 0$ (blue), 0.3, 0.5, 0.6, 0.65 (red) for a fixed $t_w = 71250$. LJ stress and covalent stress are isolated to show that the increase in yield stress is due to contributions from the covalent stress.

no hardening and results in little to no change in the yield behavior (see Fig. 4.2), rendering this effect unique to polymer glasses.

From the findings in this experiment we conclude that the enhancement in the rate of change of tensile yield stress with $t_w$ found in experiments can be attributable to the increase in projected areal bond density. This is, therefore, not a form of mechanical deformation induced "overaging" effect; the glass is not undergoing the structural recovery that leads it closer to its equilibrium. As discussed in the introduction, there are many seemingly contradictory examples of experimental findings that can be interpreted as mechanically induced rejuvenation or overaging (for example, see ref. [2]). Finding the origin behind this stress enhanced yielding behavior and verifying that it is, in fact, not an example of overaging as one may have suspected, is a significant step towards unraveling some of the existing confusions. This work should motivate future simulation work on exploring the origins of other rejuvenation and overaging examples found in experiments. The goal is to be able to determine what can be classified as true manifestations of rejuvenation and overaging, which will help greatly in the development of meaningful theories and predictions about the aging behavior in glasses.

Finally, the findings from this work are also important from an engineering perspective. As mentioned previously, realistic constitutive equations that capture the dependence of the system's yielding behavior on its thermomechanical histories are
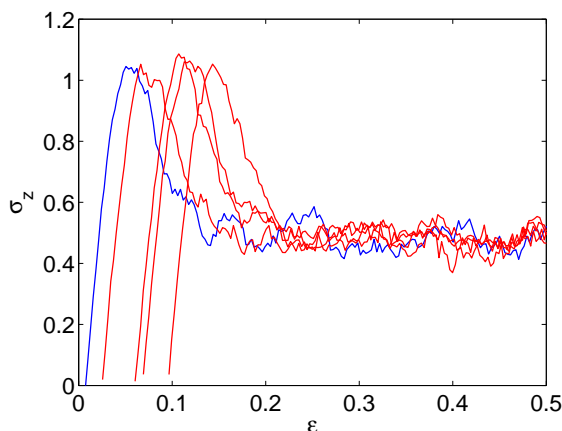
Figure 4.2: Stress-strain curves of a binary LJ system for $\sigma_0 = 0$ (blue), 0.1, 0.15, 0.2, 0.25 (red) for a fixed $t_w = 71250$ shows little change in the yield behavior.

difficult but crucial to predicting the performance of glassy systems. While it is possible to modify the existing models with parameters and shift functions such that they are able to fit experimental trends [1], this process can greatly benefit from simulation efforts that can explore the molecular origins of such trends. Specifically, now that we are able to verify that the enhancement in yield stress is proportional to molecular orientation and logarithmic time, can we explicitly account for this in the constitutive relations?

In chapter 3 we focused on the ambiguity between the two manifestations of aging: the slow logarithmic dependence of thermodynamic quantities and the power law dependence of dynamical quantities with respect to time since vitrification. While both manifestations of aging have been used extensively as ways of evaluating physical aging and structural recovery, the relation between the two is poorly understood. We addressed this by studying the effect of nanoscopic fillers on both manifestations simultaneously, as the inclusion of these fillers have been shown by experiments to lead to significant changes in the aging behavior. The study of polymer nanocomposites (PNC) is a much more recent research topic compared to the study of neat polymeric systems. Even though there has been significant research effort on PNCs in the last two decades, very limited research focused on the aging behavior of these systems, none of which are simulation works. This is unfortunate as one can greatly benefit from the use of simulations to study these systems as much of the physics in the interfacial can not be accessed easily in experiments.

We used a simulation model based on the generic bead-spring model [3] and single polygonic nanoparticles similar to one used in ref. [4] to study how the aging behavior is affected by the presense of nanoparticles. Using the parameters of the LJ potential we were able to tune the interaction between the polymer and nanoparticles. While the model was not able to produce effects on the bulk scale, we were able to observe interesting trends in the interfacial regions. It was found that the physical aging rate found from the relaxation of the per particle pair energy was reduced significantly near the attractive polymer-nanoparticle interfaces, and that this decrease was closely tracked by the reduction in mobility. Opposite but consistent trends were also found at the repulsive polymer-nanoparticle interfaces. This demonstrated that the model is able to produce enhancement/suppression of motions (in the interfacial region) that are associated with structural relaxations, resulting in the enhancement/suppression of physical aging rates as suggested by ref. [5]. However, by tracking the mean square displacement of the polymer atoms and finding the corresponding shift factors, it was found that the aging exponents are relatively unaffected by the presence of nanoparticles, and do not change measurably between the bulk and interfacial regions. The same trends were found for the aging exponents from the creep compliance curves. While this may be surprising, it is important to recognize that the aging exponent is associated with the memory of the system whereas the physical aging rate is associated with the absolute change in material properties. While the two describe very different aspects of aging, we have shown here that they are, in fact, affected very differently when subject to confinement. This work should motivate future experiments that focus on the simultaneous evaluation of the aging exponent and the aging rate as a better understanding of the relationship between the two is crucial to the understanding of physical aging in glasses.

In addition, it is important to continue to develop better and more realistic PNC models that can produce the same effects on the bulk scale as found in experiments. Studies of the effect of confinement on the glass transition temperature have suggested that chemical structure can play a significant role in the way confinement affects the properties of glassy systems [6, 7]. Therefore, one possible approach would be to include more atomistic details to the model to capture more aspects of chemical specificity (see ref. [8, 9] for examples of models containing different levels of atomic details). More details on the polymer nanoparticle interaction may also be required that can capture the characteristics and orientations of the hydrogen or ionic bonds

formed on the interfaces of real confined systems. Such additions to the model will undoubtedly result in complications, and it is important to take a systematic approach to optimize the tradeoff between the model's complexity and its ability to simulate realistic experimental settings.

The thesis presented here is concerned with the complications brought about by the lack of simple and consistent characterizations of aging. These complications are very difficult to address due to the intricate dependence of aging on many factors such as mechanical deformation, thermal treatment and confinement; and in turn, the dependence of these factors on aging. While it is clear that more research is needed, we hope this work will further motivate the use of simulations in conjunction with experiments when studying the aging behavior of glasses. The complex nature of glassy systems requires consistent explorations of quantities often not accessible to experiments in order to provide clues to the molecular origins of the observations found in experiments. At the same time, experiments are necessary to observe new trends that will require modifications on existing models, leading to more realistic simulations. Both will be crucial to the development of a unified description of physical aging in glasses.

# References

[1] E. T. J. Klompen, T. A. P. Engels, L. E. Govaert, and H. E. H. Meijer. Modeling of the postyield response of glassy polymers: influence of thermomechanical history. *Macromolecules*, 38:6997, 2005.

[2] G. B. McKenna. Mechanical rejuvenation in polymer glasses: fact or fallacy? *J. Phys.: Condens. Matter*, 15:S737–S763, 2003.

[3] K. Kremer and G. S. Grest. Dynamics of entangled linear polymer melts: a molecular dynamics simulation. *J. Chem. Phys*, 92:5057, 1990.

[4] F. W. Starr, T. B. Schroder, and S. C. Glotzer. Effects of a nanoscopic filler on the structure and dynamics of a simulated polymer melt and the relationship to ultrathin films. *J. Chem. Phys.*, 64:021802, 2001.

[5] R. Priestley, C. Ellison, L. Broadbelt, and J. M. Torkelson. Structural relaxation of polymer glasses at surfaces, interfaces, and in between. *Science*, 309:456, 2005.

[6] C. J. Ellison, M. K. Mundra, and J. M. Torkelson. Impacts of polystyrene molecular weight and modification to the repeat unit structure on the glass transition - nanoconfinement effect and the cooperativity length scale. *Macromolecules*, 38:1767, 2005.

[7] C. B. Roth and J. R. Dutcher. Glass transition temperature of freely-standing films of atactic poly(methyl methacrylate). *Eur. Phys. J. E*, 12:S103, 2003.

[8] J. Baschnagel and F. Varnik. Computer simulation of supercooled polymer melts in the bulk and in confined geometry. *J. Phys.: Condens. Matter*, 17:R851, 2005.

[9] K. Binder (Eds). *Monte carlo and molecular dynamics simulations in polymer science.* Oxford, 1995.